IDŐJÁRÁS

QUARTERLY JOURNAL
OF THE HUNGARIAN METEOROLOGICAL SERVICE

CONTENTS

****

http://www.met.hu/firat/ido-e.html

VOL. 104 * NO. 1 * JANUARY–MARCH 2000

IDŐJÁRÁS

Quarterly Journal of the Hungarian Meteorological Service

Editorial Office: P.O. Box 39, H-1675 Budapest, Hungary or
Gilice tér 39, H-1181 Budapest, Hungary
E-mail: prager@met.hu or *antal@met.hu*
Fax: (36-1) 290-7387

Subscription by

mail: IDŐJÁRÁS, P.O. Box 39, H-1675 Budapest, Hungary;
E-mail: prager@met.hu or *antal@met.hu*; *Fax: (36-1) 290-7387*

IDŐJÁRÁS

Quarterly Journal of the Hungarian Meteorological Service
Vol. 104, No. 1, January–March 2000, pp. 1–20

Statistical linkages between ENSO, NAO, and regional climate

Rita Pongrácz and **Judit Bartholy**

Department of Meteorology, Eötvös Loránd University
H-1518 Budapest, P.O. Box 32, Hungary
E-mails: prita@caesar.elte.hu; bari@ludens.elte.hu

(Manuscript received 13 July 1999; in final form 22 February 2000)

Abstract—It has been demonstrated that large scale oscillation phenomena (e.g., ENSO, NAO, PNA,...) have a great importance in influencing many climatic variables at different regions of the Earth. These phenomena do not take place independently, however, the mechanisms and interrelationships are not completely understood so far. The main idea of this paper is to describe statistical linkages between the large scale atmospheric oscillations and regional climate parameters. In order to understand the circulation and temperature structure over the Atlantic European region an analysis of atmospheric macrocirculation patterns (MCPs) is carried out via a conditional probability framework. The frequency distributions of regional MCP classes (constructed by Hess and Brezowsky, and Péczely) under different phases of large-scale oscillations are examined. Focusing on the Carpathian Basin, ENSO related regional climate analysis is carried out. Finally, lag correlation analysis are presented to compare local precipitation, regional temperature anomaly time series and different NAO indices (Jones, Hurrell, spatial SST differences).

Key-words: El Niño-Southern Oscillation, North Atlantic Oscillation, macrocirculation pattern, regional climate, statistical relationship.

1. Introduction

The El Niño phenomenon originally referred to winter-periods when cold upwelling fails to come near the South American shore at Peru and Ecuador, so unusually warm sea surface temperature (SST) occurs in the area. Another phenomenon of the tropical Pacific region is the Southern Oscillation (SO) that refers to the variability of the tropical atmosphere, namely, a large-scale fluctuation of atmospheric air mass between the Eastern and Western parts of the Pacific Ocean. Since these two phenomena have close interrelationship, a common abbreviation, ENSO (El Niño-Southern Oscillation) is widely used to

refer to a quasi-periodic redistribution of heat and momentum in the Pacific area. It involves both the atmosphere and the ocean (*Philander*, 1990).

Over much of the middle and lower latitudes of the globe, ENSO events are the most important external sources of year to year variability in climate. The interest shown in ENSO by scientists from different scientific backgrounds has increased since the 1982–83 El Niño, which has been labeled as the strongest one in the last 100 years. There was a good chance that the 1997–98 ENSO event will hit this record, but after a very intense and frightening starting period it did not. Many questions were answered in the last 10–15 years, many potential relationships that might exist between El Niño events and climate anomalies worldwide were examined and some has been proven. Let us mention here just some of them: reduced tropical cyclone activity in the western Pacific, reduced precipitation in Australia (*Nicholls* and *Kariko*, 1993), later onset of the Indian monsoon (*Joseph et al.*, 1994), increased winter rainfall in the southern United States (*Diaz* and *Markgraf*, 1992).

However, many general and specific ENSO related questions could be asked which have not been answered yet: Is it possible to link other oscillations to ENSO? Do ENSO phases have particular circulation features on MCP frequency distributions? Furthermore, the cumulative economic effects of El Niño are substantial, and there is considerable interest in understanding and predicting the occurrence and magnitude of El Niño events (*Glantz et al.*, 1987).

This paper investigates ENSO effects on tropospheric circulation and MCPs; in the following six chapters we will show selected results of our work.

2. Data

Several types of data have been used in the present paper since different kinds of analysis were completed.

Daily circulation and temperature fields from the NMC Grid Point Data Set (version III, 1996) were analyzed. This hemispherical database was composed in 1996 by the *Department of Atmospheric Sciences* at the University of Washington and the *Data Support Section* in NCAR. Height and temperature fields of several geopotential levels are available in NMC octagonal grid form (*Lenne*, 1970). The total 47 $\times$ 51 gridpoints are equally spaced when viewed on a polar stereographic grid, centered on the North Pole and rotated such that 10°E is a horizontal line to the right of the Pole. We used the following data sets: sea level pressure, 500 hPa, 700 hPa, 850 hPa geopotential heights and temperature on 500 hPa, 700 hPa and 850 hPa geopotential levels. Most of these time series consist of 33 years (1962–94) daily data fields but some of them are longer and consist of 40 years (1955–94) observations. In the present paper the original grid was converted into a latitude-longitude grid and then the Atlantic European region (30°–70°N latitude, 25°W–40°E longitude) was selected. It is represented by 63 gridpoints using 10° $\times$ 10° diamond grid resolution.

Several classifications of macrocirculation patterns (MCP) time series are available; in the present paper we will evaluate only two of them: (1) MCP defined by *Hess* and *Brezowsky* (1952, 1977) for the European continent. This dataset consists of daily HB codes from 1881 to 1997. (2) Another MCP code system was defined by *Péczely* (1961) which considers also the European weather situation particularly in the Carpathian Basin. Time series (*Péczely*, 1983; *Károssy*, 1994, 1997) include daily codes for the period 1881–1996.

Global sea surface temperature (SST) fields were obtained from *NOAA* (1997). This dataset includes daily interpolated fields of 1950–1998 with resolution of $2^\circ \times 2^\circ$ over the hemispheres. *Reynolds* and *Smith* (1994) describe optimum interpolation technique that has been applied to compose the SST dataset. Several key regions were defined based on the correlation coefficients between SST fields and climate parameters of the Carpathian Basin (*Bartholy* and *Pongrácz*, 1998a). Then, the differences between the spatial average SST values of these key regions were applied as oscillation indices.

Finally, monthly mean temperature and daily precipitation amounts measured at four meteorological stations in Hungary (Debrecen, Keszthely, Pécs, Szeged) were used as a representation of regional meteorological parameters. The precipitation time series consist of daily values from 1901 to 1994, and the temperature dataset includes monthly mean values calculated for 16 Hungarian stations for the period 1881–1994. *Fig. 1* indicates the geographical locations of the meteorological stations in Hungary that have been used in the analysis.

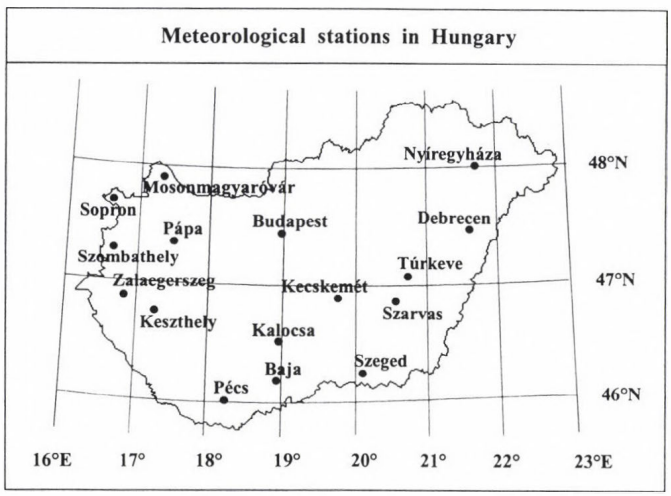

Fig. 1. Locations of the 16 Hungarian meteorological stations used in the analysis.

3. ENSO related circulation and temperature variability

Variabilities of circulation and temperature fields were examined using the available dataset listed in the previous section. EOF-analysis (*von Storch*, 1995) was applied to explore the action centers of the Atlantic European grid during the different ENSO phases (e.g., El Niño, La Niña and neutral periods). During this numerical procedure the eigenvalue equations of correlation matrices of geopotential fields have been solved. Dimension of a matrix equals to the number of gridpoints, that is 63 in this case, representing the Atlantic European region between 30°–70°N latitude and between 25°W–40°E longitude. Eigenvectors provide EOF modes corresponding to the eigenvalues, which indicate percentages of contribution to total variance of geopotential fields.

Thus, the largest positive and negative values demonstrate action centers on maps showing EOF modes. Daily geopotential height and temperature fields of several geopotential levels (AT500, AT700, AT850) were evaluated, as well as daily sea level pressure field. They all were separated into 4 seasonal time series.

First, EOF modes of circulation were calculated in the Atlantic European region during El Niño, La Niña and neutral phases (*Pongrácz et al.*, 1997). These ENSO phases were determined according to *Kiladis* and *Diaz* (1989). Contributions to total variance of the 1st, 2nd, and 3rd EOF modes are 21–26%, 16–23%, and 12–17%, respectively (*Table 1*). In case of neutral, El Niño and La Niña periods slightly larger portion of the total variance are explained by the 1st, the 2nd, and the 3rd EOF-modes, respectively, than in the other phases. The first six EOF modes usually explain the 80% of total variance, while the first nine EOF modes explain the 90%. In this paper EOF modes with the largest variances are shown and discussed.

Table 1. Contribution to total variance of 1st, 2nd and 3rd EOF modes and cumulative contributions to total variance in the case of different time series (%)

	1st EOF modes	2nd EOF modes	3rd EOF modes	The first 6 modes	The first 9 modes
Sea level pressure	23 - 25	18 - 23	13 - 17	78 - 81	87 - 90
850 hPa	22 - 26	18 - 21	12 - 18	79 - 82	89 - 91
700 hPa	21 - 25	17 - 19	12 - 17	78 - 81	89 - 91
500 hPa	21 - 23	16 - 17	12 - 16	75 - 78	87 - 89

In *Fig. 2* the 1st, 2nd and 3rd EOF modes of sea level pressure can be seen for the winter season. This figure and other results suggest that the 1st EOF modes do not significantly differ during the three ENSO phases (*Richman*,

1986). Nevertheless, higher EOF modes show considerable differences comparing El Niño, La Niña and neutral periods; especially, EOFs during La Niña differ from EOFs during El Niño or neutral phase. Positive and negative action centers change their positions during various ENSO phases.

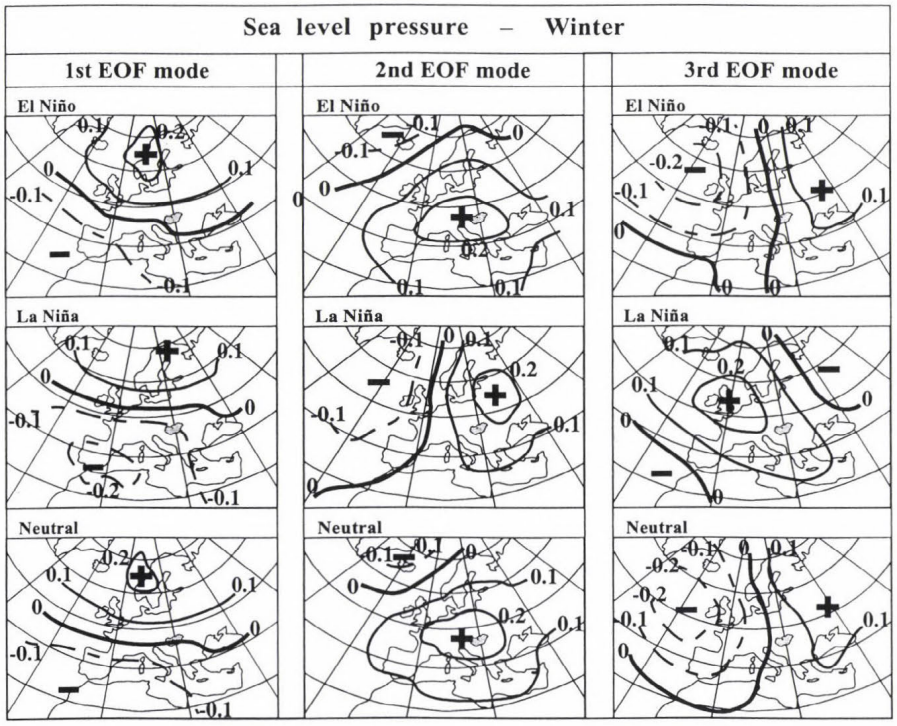

Fig. 2. 1st, 2nd and 3rd EOF modes of sea level pressure field during different ENSO phases (November–December–January, 1962–1994).

Then, EOF modes of temperature field were determined at the three geopotential levels (850 hPa, 700 hPa, 500 hPa). Their contributions to total variance of the fields are slightly smaller (by 3–4%) than in case of circulation. Since, 1st EOFs look similar during the three ENSO phases, only the 2nd EOF modes of temperature fields at 700 hPa and 850 hPa geopotential levels are shown (*Fig. 3* and *4*). The largest differences can be seen between La Niña and other ENSO phases; temperature field at 700 hPa geopotential level provides definitely more diverse structures than that at 850 hPa geopotential level. Differences between El Niño and neutral periods cannot be neglected, either,

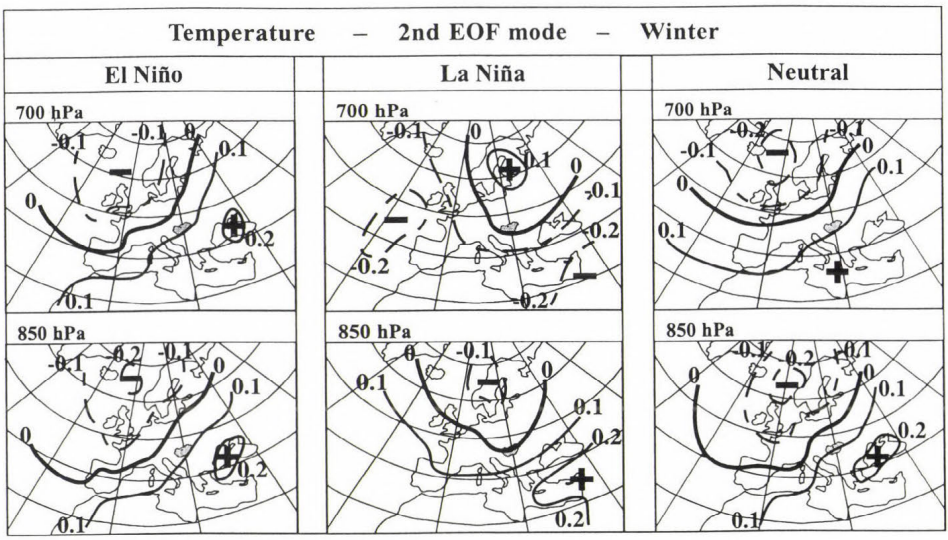

Fig. 3. 2nd EOF modes of temperature field at 700 hPa and 850 hPa geopotential levels during different ENSO phases (November–December–January, 1962–1994).

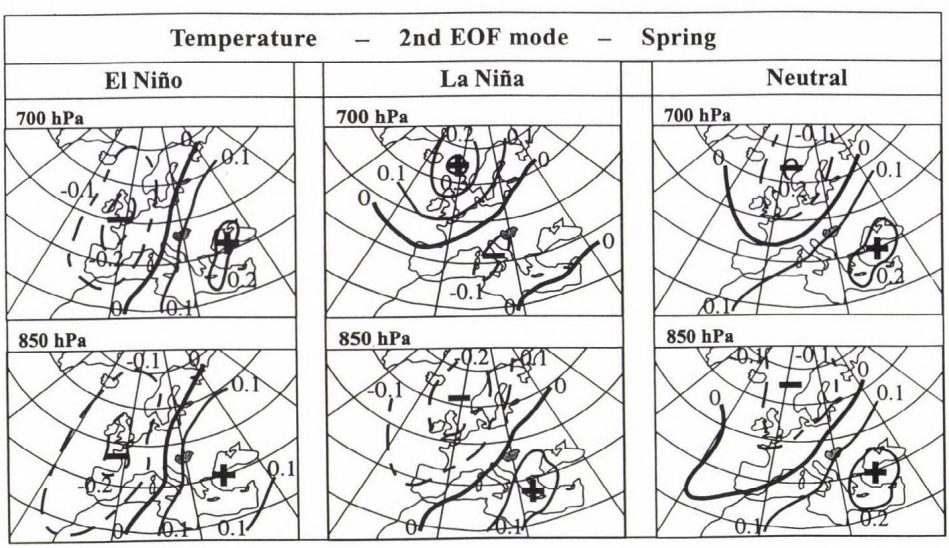

Fig. 4. 2nd EOF modes of temperature field at 700 hPa and 850 hPa geopotential levels during different ENSO phases (February–March–April, 1962–1994).

although they are smaller than in case of La Niña periods. During both season various levels provide similar structures in case of the 2nd and 3rd (not shown in this paper) EOF modes. Nevertheless, it is important to note that during La Niña events this latter statement is not true; more analysis should be made in the future hoping to get more information about the reasons.

The above results of this EOF analysis suggest that ENSO signals have considerable effects on the climate of the Atlantic European region. Further evaluation are planned to compare EOFs on several geopotential levels to the results of singular vector analysis (e.g., *Buizza* and *Palmer*, 1995; *Buizza et al.*, 1997).

Composite temperature and geopotential height anomaly fields were calculated and mapped for the different ENSO phases in the winter key-period, and also with a seasonal lag in spring. For both periods, temperature and circulation patterns present major differences during El Niño and La Niña events. As an illustration temperature anomaly fields are shown at two different geopotential levels during spring (*Fig. 5*). The results suggest that geopotential levels do not affect anomaly fields considerably. However, different ENSO phases provide reverse structures of temperature anomaly.

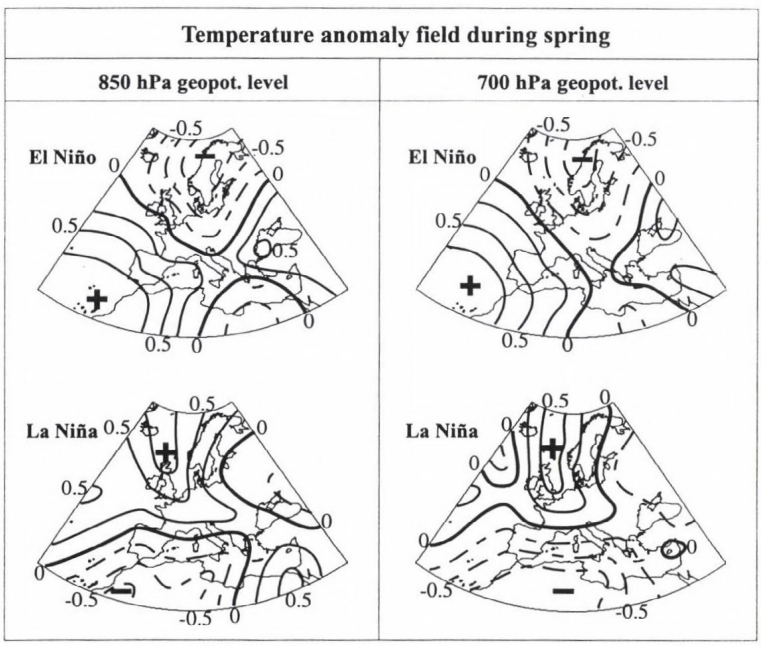

Fig. 5. Anomaly fields of temperature at 700 hPa and 850 hPa geopotential levels during different ENSO phases (February–March–April, 1962–1994).

4. ENSO related changes in regional circulation patterns

As Hungary is located in the Central European region, we focused the ENSO-related investigation to this area.

Effects of different ENSO events on regional circulation structures of the Atlantic European region were examined using the *Hess–Brezowsky* circulation types (1952, 1977). The available dataset consists of daily MCP codes from 1881 to 1997 for Western and Central Europe. To find the major components of ENSO phases on regional features of circulation, it was necessary to aggregate the original 29 HB types into groups. The characteristics of the classification are summarized and described in *Table 2*.

Table 2. Macrocirculation types defined in the Hess-Brezowsky system

Circulation type	Main flow direction	Macrosynoptic type (notation)
Zonal	West (W)	West anticyclonic (Wa) West cyclonic (Wz) Southern West (Ws) Angleformed West (Ww)
Half-meridional	Southwest (SW)	Southwest anticyclonic (SWa) Southwest cyclonic (SWz)
	Northwest (NW)	Northwest anticyclonic (NWa) Northwest cyclonic (NWz)
	Central European high (HM)	Central European high (HM) Central European ridge (BM)
	Central European low (TM)	Central European low (TM)
Meridional	North (N)	North anticyclonic (Na) North cyclonic (Nz) North, Iceland high, anticyclonic (HNa) North, Iceland high, cyclonic (HNz) British Islands high (HB) Central European Trough (TRM)
	Northeast (NE)	Northeast anticyclonic (NEa) Northeast cyclonic (NEz)
	East (E)	Fennoscandian high anticyclonic (HFa) Fennoscandian high cyclonic (HFz) Norwegian Sea – Fennoscandian high anticyclonic (HNFa) Norwegian Sea – Fennoscandian high cyclonic (HNFz)
	Southeast (SE)	Southeast anticyclonic (SEa) Southeast cyclonic (SEz)
	South (S)	South anticyclonic (Sa) South cyclonic (Sz) British Islands low (TB) Western European Trough (TRW)

One aspect for making groups was the dominant direction of air mass movements (*Bartholy* and *Pongrácz*, 1998b). According to the main air flow directions (W, SW, NW, N, NE, E, SE, S), eight different groups and two extra classes where the circulation is controlled by Central European pattern were selected. Furthermore, circulation characteristics could be another factor, thus zonal, half-meridional and meridional MCP classes were defined. Zonal MCP class includes 4 HB types, meridional MCP class consists of 18 different HB types, and the other 7 HB types compose the half-meridional MCP class. Finally, cyclonic and anticyclonic MCP classes were separated. These MCP classes containing several HB types were statistically studied, namely, their empirical relative frequencies were compared and evaluated during El Niño, La Niña and neutral periods.

First, the intensification of ENSO effects on the European macrocirculation was tested. According to our hypothesis, the effects became more intense during the last 40–50 years than they were before. This idea is supported by the comparison of relative frequencies of MCP classes in the entire time series (1881–1997) and the last 43 years (1955–1997). Furthermore, since ENSO seems to have dynamic and global circulation-related reasons (*Cane*, 1992), the macrocirculation of various areas, like the Atlantic European region, must be affected by the intensification. The changes in frequencies of MCP classes characterized by their main direction were compared during the last 117 years (1881–1997) and the last 43 years (1955–1997) during El Niño and La Niña phases in the key ENSO periods, winter and spring (*Fig. 6*). Our results suggest that relative frequencies of MCP classes changed considerably greater (4–5 times in some cases) during the last 43 years than during the longer 117 year long period. Furthermore, in general, both in winter and spring the changes in frequencies of MCP classes occurred with opposite sign during El Niño and La Niña phases. Note that the frequency of MCP classes with eastern flow decreased during La Niña winters (North-Eastern flow: by 78%, Eastern flow: by 42%, South-Eastern flow: by 77%). While La Niña springs can be characterized by enhanced frequency of eastern MCP classes (especially North-Eastern flow), El Niño springs were dominated by diminished frequency of these MCP classes. Finally, the occurrence of the North-Western types increased by 108% during La Niña winters and by only 20% during El Niño winters.

Next, changes in occurrences of the three different circulation characteristics were evaluated during ENSO phases. *Fig. 7* shows how the relative frequency of zonal, half-meridional and meridional MCP classes changed during El Niño and La Niña events comparing the four seasons of the last 43 years. Major changes occurred in winter in case of La Niña phase, namely, meridional circulation decreased while zonal circulation increased by about 21–22%. The greater effect of ENSO phenomema on circulation of the autumn season occurred during El Niño periods: frequency of zonal MCP classes decreased by 22%, and meridional MCP classes increased by 28%. Both El Niño and La

Niña phases affected the circulation of Western and Central Europe in spring: zonal MCP classes increased considerably during El Niño periods, while half-meridional MCP classes decreased and meridional MCP classes increased during La Niña phase.

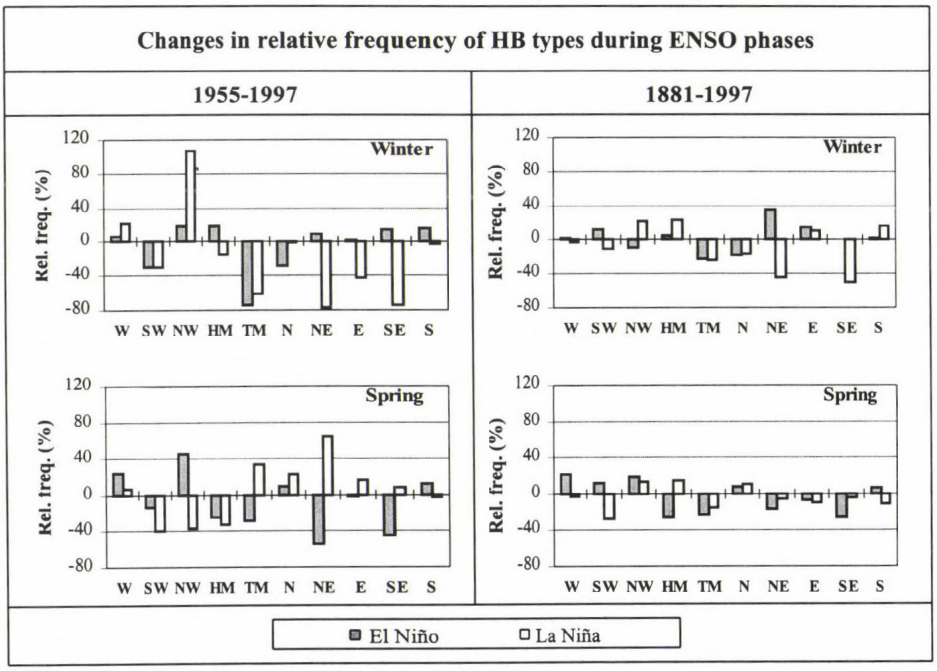

Fig. 6. Changes in relative frequency of MCP classes during ENSO phases in winter and spring in the last 117 years and 43 years.

The major (frequently exceeding 20%) changes in occurrence of MCP classes suggest significant changes in regional temperature and precipitation patterns.

Finally, we studied cyclonic and anticyclonic MCP classes (*Fig. 8*). Effects of ENSO phases on frequencies of cyclonic and anticyclonic circulation patterns in winter and summer were not significant. The largest changes occurred during spring: cyclonic dominance increased and anticyclonic dominance decreased by 28% during El Niño events in the last 43 years. La Niña periods had opposite but slightly smaller effect on the relative frequency of cyclonic and anticyclonic MCP classes. Changes in autumn are still considerable and contrary but weaker than in spring, especially during El Niño years.

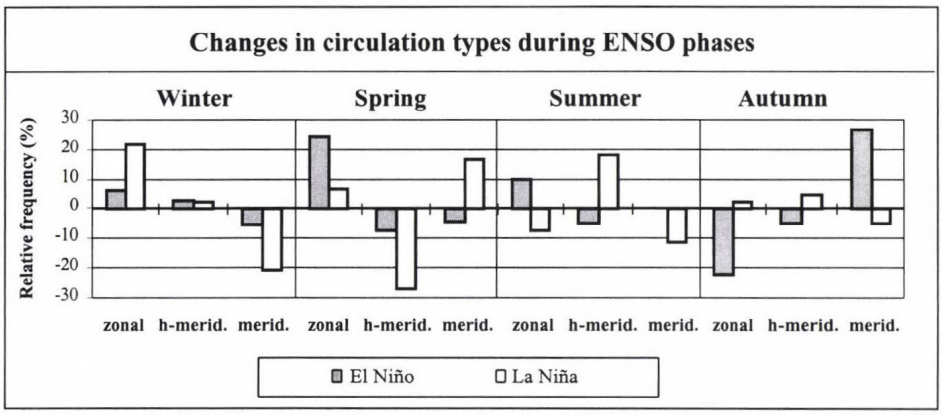

Fig. 7. Changes in circulation types during different ENSO phases (1955–1997).

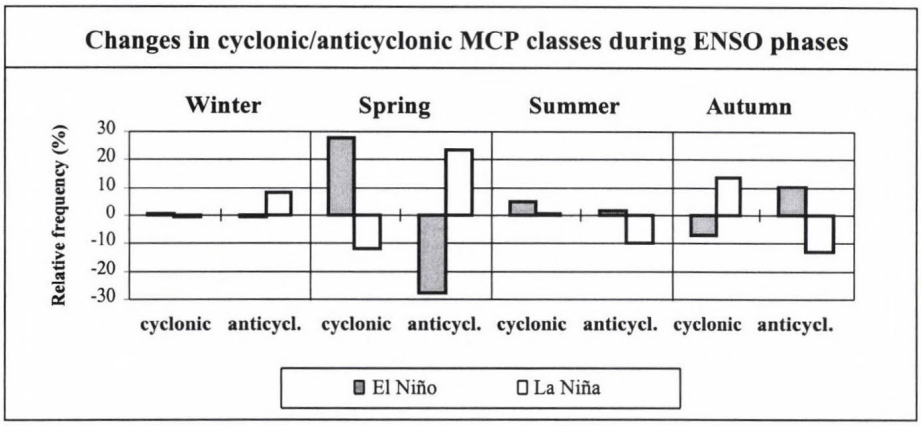

Fig. 8. Changes in frequencies of cyclonic/anticyclonic circulation patterns during different ENSO phases (1955–1997).

Relative frequencies of cyclonic and anticyclonic *Péczely*-MCP classes (1961) which provide circulation features focused mainly on the Carpathian Basin show similar changes during El Niño events: the largest changes occurred in spring (*Fig. 9*). Since HB types consider larger area than Péczely types the changes are greater, as well. During La Niña events both cyclonic and anticyclonic MCP classes (in the Péczely system) possess minor changes in spring and autumn. However, in the winter and the summer months relative

frequency changes vary between 10–25% during La Niña events, occurrences of cyclonic MCP classes changed more considerably than those of anticyclonic MCP classes.

Analysis presented in this paper show that macrocirculation patterns significantly differ in the Atlantic European region during El Niño and La Niña periods.

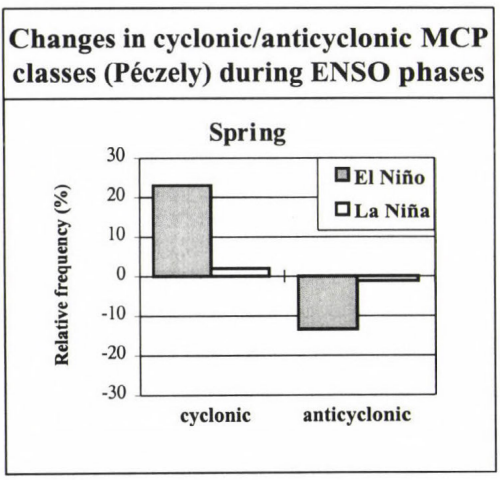

Fig. 9. Changes in frequencies of cyclonic/anticyclonic circulation patterns (defined by Péczely) during different ENSO phases (1955–1996).

5. ENSO related regional climate analysis

In this part of our study the most anomalous periods of the year were selected and investigated for the different ENSO episodes. In order to fulfill this task standard deviations of regional monthly temperature and precipitation values were calculated besides the average anomalies (*Fig. 10*). Large negative temperature anomalies were present during El Niño winters (from December to March), while warmer conditions were more likely to occur in May-June during La Niña phase. La Niña springs (from February to April) are indicated by colder climate conditions. Furthermore, our analysis suggest that La Niña episodes affect the regional monthly precipitation more than El Niño. Large negative precipitation anomalies occurred in October and November, and wetter conditions were likely to be observed in April and August.

These results are mostly supported by our findings when monthly values of standard deviation were taken into consideration. In some cases, for example during El Niño episodes, precipitation anomalies in October are close to 0; on the other hand, the standard deviation is one of the largest during El Niño years. The explanation can be clear, namely, the large anomalies with different

signs eliminate one another. Furthermore, average precipitation anomaly is quite large with little deviation during La Niña episodes. The corresponding distributions of anomalies are presented in *Fig. 11* (right panel). Note the different histograms and fitted curves for the different ENSO phases; large positive anomalies (> 40 mm) disappeared during La Niña and increased during El Niño. Chi-square test for homogeneity was carried out pairwise and the results show differing empirical distributions at 0.05 significance level in each pair.

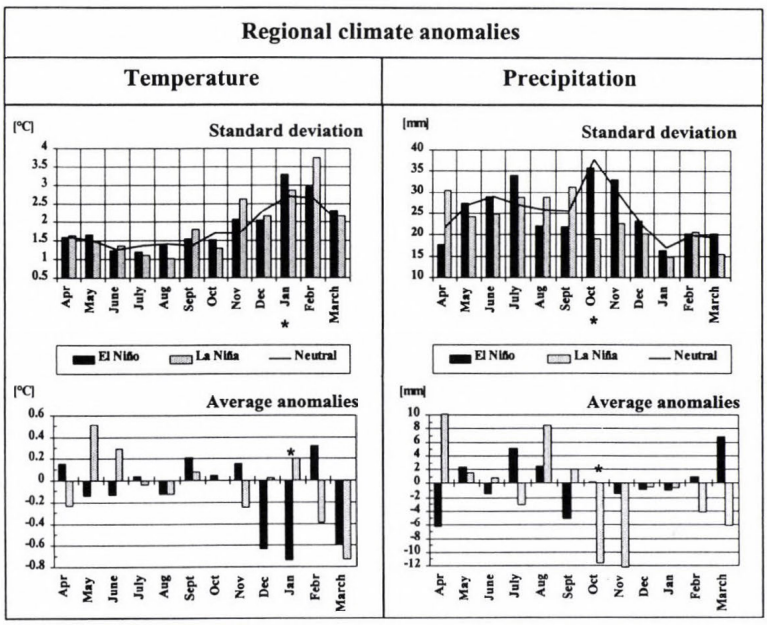

Fig. 10. Standard deviation and average of anomalies of regional climate parameters (temperature and precipitation, based on 16 Hungarian meteorological stations) during different ENSO phases.

Another example can be the temperature anomalies in January: the largest negative anomaly occurred on average during El Niño episodes with high standard deviation, while La Niña can be characterized by slightly less standard deviation, so anomalies eliminate each other (similarly to the precipitation in October during El Niño). Thus, histograms of January temperature anomalies during El Niño, La Niña and neutral phases show significantly different distributions (Fig. 11, left panel): colder than average conditions are more likely to occur during El Niño than during neutral years, while extremely cold

and warmer than average conditions occurred during La Niña. Similarly to the precipitation case, chi-square tests for homogeneity show differing empirical distributions at 0.05 significance level pairwise.

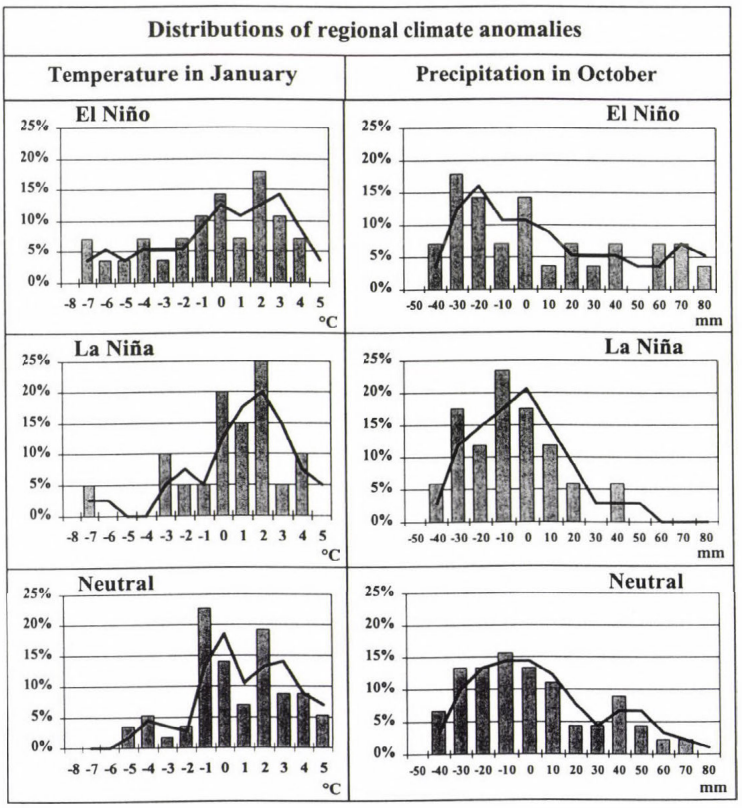

Fig. 11. Empirical distributions of regional temperature (in January) and precipitation anomalies (in October) during ENSO phases.

Relative frequencies of outliers of regional climate parameters were determined during different ENSO phases in each month (*Table 3*). A temperature or precipitation anomaly was considered as an outlier if it is out of the $[-\sigma;\sigma]$ or the $[-1.5\sigma;1.5\sigma]$ interval. In the case of precipitation the wider interval results less (half-third) negative outlier frequencies than positive ones since the distribution of precipitation cannot be estimated by normal but gamma distribution skewed in positive anomalies (*Wilks*, 1995).

Table 3. ENSO related frequencies (%) of regional temperature and precipitation outliers (considering $[-\sigma;\sigma]$ and $[-1.5\sigma;1.5\sigma]$ intervals)

Climate variable	ENSO phase	$[-\sigma;\sigma]$		$[-1.5\sigma;1.5\sigma]$	
		+	−	+	−
Temperature	El Niño	15.9	17.7	6.2	9.1
	La Niña	15.9	15.9	6.8	6.8
	Neutral	15.7	14.7	5.8	6.9
Precipitation	El Niño	17.6	14.3	8.9	3.6
	La Niña	14.7	16.2	9.8	3.9
	Neutral	15.5	15.1	8.8	3.4

Although the differences in annual average frequencies are small in general, the monthly values differ considerably (*Fig. 12* and *13*). However, El Niño episodes show the largest differences compared to other ENSO phases, both temperature and precipitation anomalies. Fig. 12 presents outlier occurrences of regional precipitation during ENSO episodes; La Niña years provide more diverse annual frequency distribution than El Niño: the summer half-year (April through September) is dominated by positive outliers, while negative outliers were more likely to occur (18–24%) during the winter half-year (from September to March). Positive outliers were slightly more frequent in El Niño years than negative outliers overall. Large differences occurred between positive and negative outlier frequencies, however, e.g., in August and March.

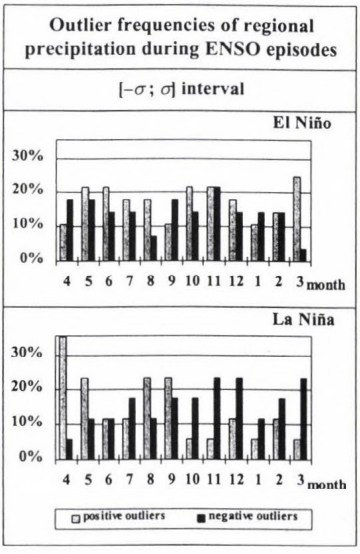

Fig. 12. Outlier frequencies of regional precipitation anomalies during ENSO episodes.

Fig. 13 compares the outlier frequencies of regional temperatures during ENSO phases considering $[-\sigma;\sigma]$ and $[-1.5\sigma;1.5\sigma]$ intervals. Outliers of the $[-\sigma;\sigma]$ interval can be defined as "not average" values, while outliers of $[-1.5\sigma;1.5\sigma]$ as "extreme". Some major differences can be noticed in Fig. 13:

1. Neutral phase provides less diverse annual variability than El Niño or La Niña years, in both intervals.
2. While negative outliers were dominant in February-March-April during La Niña episodes in case of $[-\sigma;\sigma]$ interval, the entire winter half-year was dominated by extremely cold conditions.
3. Very high and steady frequencies of positive temperature outliers were present for both intervals in May and June during La Niña.
4. In both intervals during El Niño the negative outliers were dominant in the December-March period.

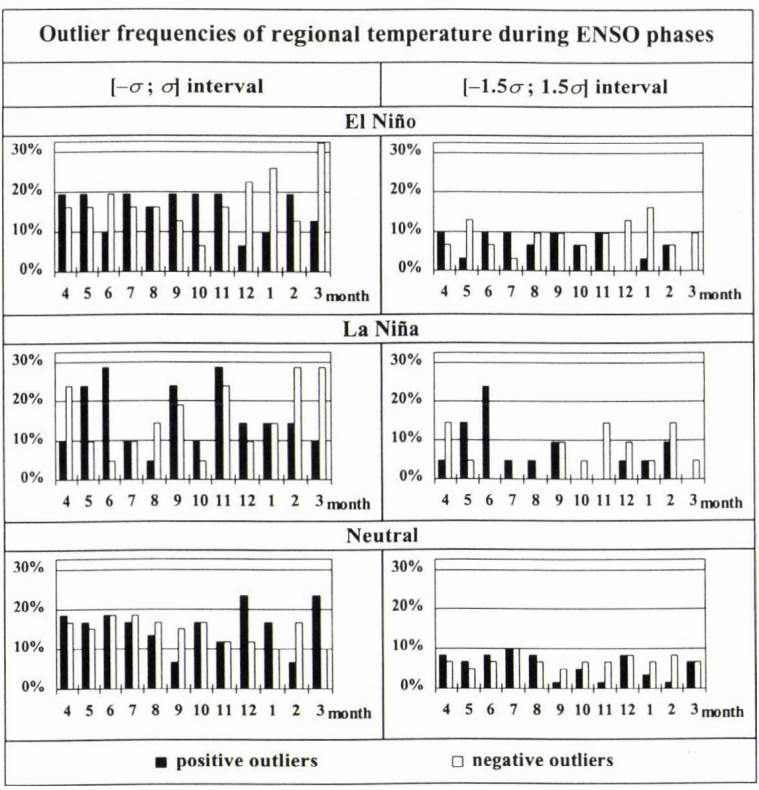

Fig. 13. Comparing outlier frequencies of regional temperature anomalies during ENSO phases.

6. Joint ENSO and NAO forcing on regional climate

While ENSO are mostly tropical phenomena, the North Atlantic Oscillation (NAO) is one of the large-scale modes of climate variability on extratropics that is most pronounced during winter (*Wallace* and *Gutzler*, 1981). As the name indicates, the NAO is centered on the North Atlantic Ocean basin. The Icelandic low-pressure center tends to be lower than normal, while the high-pressure center near the Azores tends to be higher than normal and vice versa (*Barnston* and *Livezey*, 1987). Both ENSO and NAO are oscillations with different amplitudes and they have some quasi-periodic features. In this part of our research we examined their interference and their joint regional impact on temperature and precipitation observed in the Carpathian Basin with a teleconnection study.

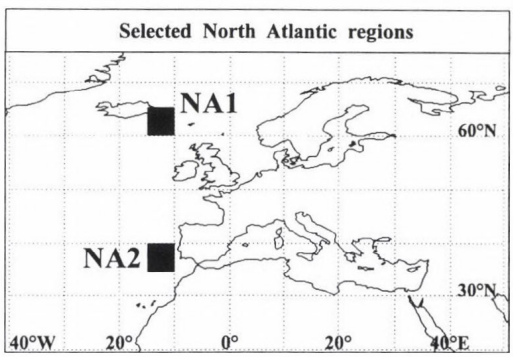

Fig. 14. Key regions for NAO index. NA1: 65°–60°N, 15°–10°W; NA2: 40°–35°N, 15°–10°W.

NAO was represented by the time series of the difference between SST values averaged on two selected regions of the North Atlantic ocean (*Fig. 14*). Locations of sectors NA1 (eastward from Iceland) and NA2 (Azori Islands) are traditionally used for investigating the general characteristics of NAO (e.g., *Hurrell*, 1995). In these sectors spatial average of SST values were calculated for each month, 1950–1998. Annual teleconnection analysis was carried out on this NAO index and on temperature/precipitation time series for the Central European region during different ENSO phases. In order to consider the wave effect of the oscillations, several months pre- and post-lag were included in the study. Although lag correlation coefficients were calculated for the entire [–12 months; +12 months] interval we present 0–9 month pre-lag correlations here since this period can be considered physically reasonable (*Glantz et al.*, 1991). *Fig. 15* presents lag correlation coefficients between NAO index (based on SST) and regional climate parameters observed in December and February during ENSO episodes. These two months are shown here because NAO is the

most pronounced during the winter season. Large differences can be seen in correlations between NAO and meteorological characteristics during El Niño and La Niña periods. In general, absolute values of correlation coefficients are higher during La Niña than during El Niño years; it can be partly explained by less La Niña events in the period studied here than El Niño events. However, since other results of our analysis provided similar conclusions, La Niña years undoubtedly tend to affect the regional climate parameters more than El Niño episodes. Furthermore, note the changing signs of strong correlations, especially temperature in December and precipitation in February during La Niña events. Our study suggest that NAO and regional climatology show considerable lag (1–3 months) since simultaneous NAO index and regional temperature/precipitation values do not result in the strongest correlations.

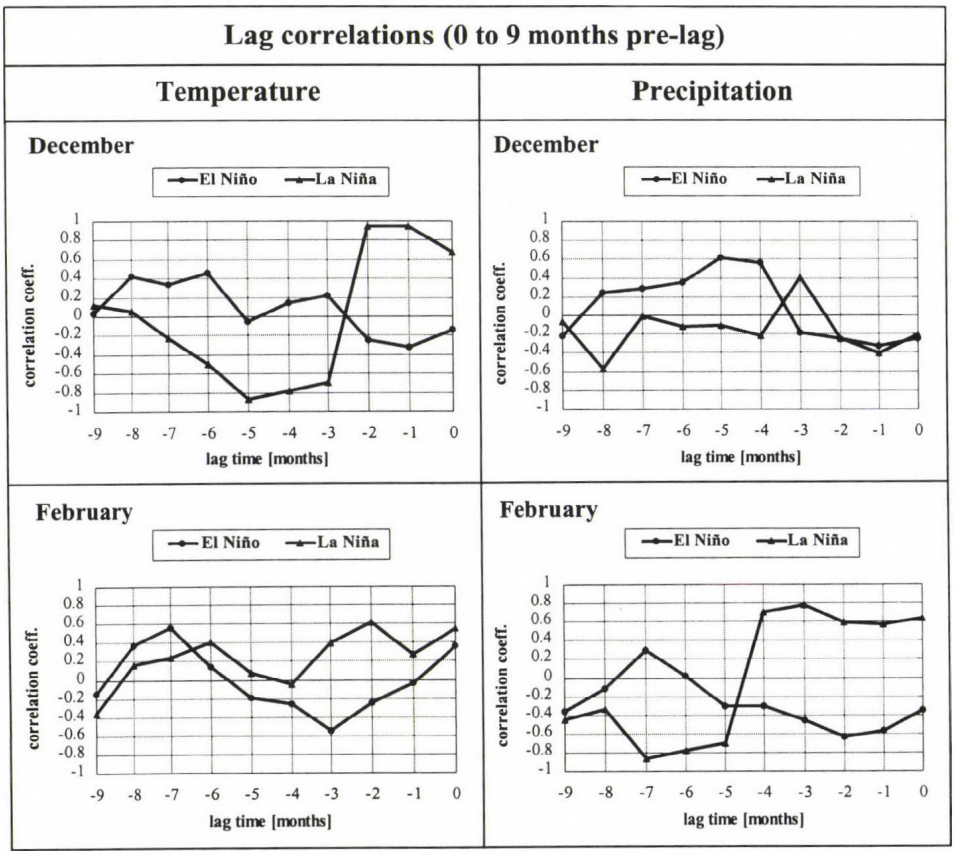

Fig. 15. Lag correlations between NAO index and regional climate parameters during El Niño and La Niña periods.

7. Conclusions

As a summary, it can be concluded that correlation analysis, EOF and other classification techniques seem to be an appropriate methodology for evaluating the impact of interannual oscillations (e.g., ENSO, NAO) on regional climate. Analyzing geopotential height fields, MCPs and global SST fields we did get stronger ENSO signals for the Central European region than in the case of secondary derived quantities (e.g., time series of SOI).

EOF modes of tropospheric circulation and temperature variability differ during the different ENSO episodes: positive and negative action centers change their positions in the case of 2nd and 3rd modes. The largest differences occurred between La Niña and other ENSO phases.

Temperature anomaly fields show reverse structure in the Atlantic European region during El Niño and La Niña episodes.

Considerable changes can be found in MCP empirical frequencies during El Niño and La Niña periods: changes in circulation character, in cyclonic/anti-cyclonic dominancy and in ENSO phase intensity. The largest changes in zonal circulation types occurred during El Niño springs and La Niña winters. Frequency of meridional MCP classes shows large decreases during El Niño autumns and La Niña winters, while half-meridional MCP classes decreased the most during La Niña springs. Changes in empirical frequencies of cyclonic and anticyclonic MCP classes are the most dominant in El Niño springs.

Outlier and anomaly statistics of regional precipitation and temperature differ considerably during El Niño and La Niña episodes. Specifically, La Niña autumns are dominated by large negative anomalies in precipitation, while wet conditions occur in La Niña April. Furthermore, cold conditions are present during El Niño winters and positive temperature anomalies in La Niña May-June.

Joint ENSO and NAO forcing seemed to affect regional climate parameters, especially during La Niña episodes. The 1–3 months lag period resulted in the most dominant relationship.

Acknowledgements—Research leading to this paper has been supported by the *Hungarian National Science Research Foundation* under grants T26629, T25803 and T15707, also, by the *Hungarian Higher Education Support Program* under grant FKFP-0193. Furthermore, the authors thank to the three unknown referees for their useful comments.

References

Barnston, A.G. and *Livezey, R.E.*, 1987: Classification, seasonality and persistence of low-frequency atmospheric circulation patterns. *Mon. Wea. Rev. 115*, 1083–1126.

Bartholy, J. and *Pongrácz, R.*, 1998a: Comparing ENSO related PNA and NAO signals. *Presentation on 7th International Meeting on Statistical Climatology*. Whistler, British Columbia, Canada, May 25-29, 1998.

Bartholy, J. and *Pongrácz, R.*, 1998b: Comparing Signals of ENSO and NAO for Selected Regions of the Northern Hemisphere. *Annales Geophysicae, Suppl. Vol. 16,* C698.

Buizza, R. and *Palmer, T.N.*, 1995: The singular-vector structure of the atmospheric global circulation. *J. Atmos. Sci. 52*, 1434–1472.

Buizza, R., Gelaro, R., Molteni, F. and *Palmer, T.N.*, 1997: The impact of increased resolution on predictability studies with singular vectors. *Quart. J. Roy. Meteorol. Soc. 123*, 1007–1033.

Cane, M.A., 1992: Tropical Pacific ENSO Models: ENSO as a mode of the coupled system. In *Climate System Modeling* (ed.: *K.E. Trenberth*). Academic Press, New York. 583-614.

Dept. of Atmospheric Sciences, Univ. of Washington and *Data Support Section, NCAR*, 1996: *NMC Grid Point Data Set* (version III).

Diaz, H.F. and *Markgraf, V.* (eds.), 1992: *El Niño: Historical and Paleoclimatic Aspects of the Southern Oscillation*. Cambridge University Press, New York.

Glantz, M.H., Katz, R.W. and *Krenz, M.*, 1987: *Climate Crisis: The Societal Impacts Associated with the 1982-83 Worldwide Climate Anomalies*. NCAR, Boulder.

Glantz, M.H., Katz, R.W. and *Nicholls, N.* (eds.), 1991: *Teleconnections Linking Worldwide Climate Anomalies*. Cambridge University Press, New York.

Hess, P. and *Brezowsky, H.*, 1952: Katalog der Grosswetterlagen Europas. *Berichte das Deutschen Wetterdienstes in der US Zone. 33*. Bad Kissingen.

Hess, P. and *Brezowsky, H.*, 1977: Katalog der Grosswetterlagen Europas. *Berichte das Deutschen Wetterdienstes. 113*. Offenbach.

Hurrell, J.W., 1995: Decadal trends in the North Atlantic oscillation regional temperatures and precipitation. *Science 269*, 676–679.

Joseph, P.V., Eischeid, J.K. and *Pyle, R.J.*, 1994: Interannual variability of the onset of the Indian summer monsoon and its assotiation with atmospheric features, El Niño, and sea surfaces temperatures anomalies. *J. of Climate 7*, 81–105.

Károssy, Cs., 1994: Péczely's classification of macrosynoptic types and the catalogue of weather situations (1951-1992). In *Light trapping of insects influenced by abiotic factors. Part I.* (ed.: *L. Nowinsky*). Savaria University Press, Szombathely, 117-130.

Károssy, Cs., 1997: Catalogue of Péczely's macrosynoptic weather situations (1993-1996). In *Light trapping of insects influenced by abiotic factors. Part II.* (ed.: *L. Nowinsky*). Savaria University Press, Szombathely, 159-162.

Kiladis, G.N. and *Diaz, H.F.*, 1989: Global climatic anomalies associated with extremes of the Southern Oscillation. *J. of Climate 2*, 1069–1090.

Lenne, R.L., 1970: *The NMC Octagonal Grid*. NCAR, Boulder, Colorado.

NOAA, 1997: *SST database*. ftp://nic.fb4.noaa.gov/ocean/clim1.

Nicholls, N. and *Kariko, A.*, 1993: East Ausrtralian rainfall events: interannual variations trends and relationships with the Southern Oscillation. *J. of Climate 6*, 1141–1152.

Péczely, Gy., 1961: *Characterising the Meteorological Macrosynoptic Situations in Hungary* (in Hungarian). Orsz. Meteorol. Int. Kisebb Kiadványai 32, Budapest.

Péczely, Gy., 1983: *Catalogue of Macrosynoptic Situations of Hungary in Years 1881–1983* (in Hungarian). Orsz. Meteorol. Szolg. Kisebb Kiadványai 53, Budapest.

Philander, S.G.H., 1990: *El Nino, La Nina, and the Southern Oscillation*. Academic Press, New York.

Pongrácz, R., Bartholy, J., Matyasovszky, I. and *Bogárdi, I.*, 1997: Relations between El Nino/La Nina Events and Large-scale Circulation Variations. *Annales Geophysicae, Suppl. Vol. 15*, C476.

Reynolds, W.M. and *Smith, T.M.*, 1994: Improved global sea surface temperature analyses. *J. of Climate 4, 929–948.*

Richman, M.B., 1986: Rotation of principal components. *J. Climatol. 6, 293–335.*

von Storch, H., 1995: Spatial patterns: EOFs and CCA. In *Analysis of Climate Variability* (eds.: *H. Storch* and *A. Navarra*. Springer-Verlag, Berlin, 227–257.

Wallace, J.M. and *Gutzler, D.S.*, 1981: Teleconnections in the geopotential height field during the Northern Hemisphere. *Mon. Wea. Rev. 109*, 784–812.

Wilks, D.S., 1995: *Spatial Methods in the Atmospheric Sciences*. Academic Press, London.

IDŐJÁRÁS

Quarterly Journal of the Hungarian Meteorological Service
Vol. 104, No. 1, January–March 2000, pp. 21–41

The land-surface model family SURFMOD

Ferenc Ács[1], **Michael Hantel**[2] and **Johann Unegg**[2]

[1]*Department of Meteorology, Eötvös Loránd University,*
H-1117 Budapest, Pázmány Péter sétány 1/A, Hungary,
E-mail: acs@caesar.elte.hu

[2]*University of Vienna, Hohe Warte 38, A-1190 Vienna, Austria*

(Manuscript received 9 April 1999; in final form 5 January 2000)

Abstract—The land-surface model family SURFMOD (**Sur**face **F**lux **Mod**el), designed jointly at the Universities of Eötvös Loránd and Vienna, is briefly considered. The attention is paid to the comparison of the most complex Psi1-PROGSURF (**Prog**nosis of **Sur**face **F**luxes) and the simpliest Pm-PTSURF (**P**riestley **T**aylor **Sur**face **F**luxes) modes. Pm-PTSURF is not only simple with respect to Psi1-PROGSURF but also it is extremely simple with respect to other biophysical models.

In the preliminary tests on the Cabauw data set it has been shown that

- both modes reproduce satisfactorily the observed annual mean values, seasonal changes and the instantaneous values of turbulent and water fluxes,
- Pm-PTSURF is able to capture—though its extreme simplicity—the governing processes at Cabauw site: the potential evapotranspiration $E(\theta_S)$ governed by atmospheric conditions and
- the simulation results of Psi1-PROGSURF and Pm-PTSURF do not deviate from each other in a great extent since there is no great deviation between their $E(\theta_S)$ parameters.

The results obtained are relevant to the Project for Intercomparison of Land-Surface Parameterization Schemes. SURFMOD is an effective tool in performing comparative studies. Presently it is also used to specify the boundary conditions for the software DIAMOD which is routinely used at the University of Vienna to diagnose the convective fluxes in the free atmosphere.

Key-words: model family, intercomparison of models, complexity versus simplicity.

1. Introduction

The land-surface model family SURFMOD, designed jointly at the Universities of Vienna and Eötvös Loránd, consists of three model family members (see *Table 1*): the PROGSURF (**Prog**nosis of **Sur**face **F**luxes), the PMSURF (**P**enman-**M**onteith **Sur**face **F**luxes) and the PTSURF (**P**riestley **T**aylor **Sur**face

Fluxes). PROGSURF is based on the work of Budapest-Vienna working group (*Ács*, 1995; *Ács et al.*, 1996) and on the previous work of *Ács et al.* (1991) and *Ács* (1994). The most complete description and analysis of PROGSURF is given in *Ács* and *Hantel* (1998a). On the basis of this publication we can qualify PROGSURF as PILPS model[1]. The complete documentation of PROGSURF's source code in a form of a User Manual is also given in *Ács et al.* (1998a). This User Manual enables us to use the PROGSURF not only for scientific but also for educational purposes.

Table 1. SURFMOD family members and modes and their main characteristics

SURFMOD family members and modes			
Family member	Mode	Description	Details
PROGSURF	Psi1	F_{ad} is parameterized fully and F_{ma} by leaf water potential	*Ács* and *Hantel* (1998a)
	Psi2	$F_{ad} \equiv 1$ and F_{ma} is parameterized by leaf water potential	*Ács* and *Hantel* (1998a)
	Theta	F_{ad} is parameterized fully	*Ács* and *Hantel* (1998a) *Ács* and *Hantel* (1998b)
	Combi-nation	LE is parameterized by PM combination equation and H by aerodynamic formula	*Ács* (2000)
PMSURF	Ps1	F_{ma} is parameterized by leaf water potential	*Ács* and *Hantel* (1999)
	Theta	F_{ma} is parameterized by soil moisture	
PTSURF	Prog	LE is parameterized by Priestley-Taylor formula and H by aerodynamic formula	
	Pm	LE is parameterized by Priestley-Taylor formula and H as the residual term from the energy balance equation	

Symbols: F_{ad} – atmospheric demand function in the canopy resistance parameterization, F_{ma} – moisture availability function in the canopy resistance parameterization, LE – latent heat flux and H – sensible heat flux

To investigate the model optimizing problems in scope of PILPS, we replaced PROGSURF's aerodynamic formulas for turbulent flux parameterization by the Penman-Monteith approach (*Monteith*, 1965; *Dolman*, 1993; *Monteith*, 1995). This reformulation of PROGSURF occured in 1997; the model

[1] Project for Intercomparison of Land-Surface Parameterization Schemes

model obtained (referred to as PMSURF) can be treated either as a new model or as a specific model version of PROGSURF. We chose the latter case. A detailed description of PMSURF in comparison to PROGSURF is presented in *Ács* and *Hantel* (1999). Analogously to PROGSURF, there is also a User Manual for PMSURF (*Ács et al.*, 1998b). PTSURF is constructed at the end of 1998 and at the beginning of 1999. It can be treated as a Priestley-Taylor formula based PROGSURF or PMSURF. The only difference between PROGSURF/PMSURF and PTSURF is in the parameterization of latent heat flux. PROGSURF or PMSURF uses the gradient formula or the Penman-Monteith's formula while PTSURF uses the Priestley-Taylor formula. PTSURF's User Manual is not available, but it can be treated as a documented model since its many parts are very similar to the PROGSURF and/or PMSURF.

Two basic facts are valid concerning PILPS:

- the scatter of results obtained by different land-surface parameterization schemes is enormously great for all tested climate regimes (*Shao* and *Henderson-Sellers*, 1996), and
- the analysis of the causes of deviations are sporadic or completely missing.

In this study, using SURFMOD as an effective tool for performing comparative studies, we try to contribute to PILPS considering following objectives:

1. We describe, validate and compare the most complex (Psi1-PROGSURF) and the simpliest (Pm-PTSURF) modes of SURFMOD. The models are run in off-line mode using Cabauw data set.
2. We show for the Cabauw data set that the very simple Pm-PTSURF mode is capable to capture the governing processes and even it yields the most favorable results with respect to some most complex SURFMOD modes.
3. We show the reasons why the very simple Pm-PTSURF can reproduce the main effects.

2. The SURFMOD model family

SURFMOD's input data are: model constants, initial values of prognostic variables (shortly referred to as initial conditions), variable land-surface parameters and atmospheric forcing data. SURFMOD's outputs are: instantaneous and daily, monthly and yearly averaged energy and water fluxes. SURFMOD's family members and modes can use different initial conditions and atmospheric forcing data. An overview of used initial conditions and atmospheric forcing data is given in *Table 2a* and *2b*, respectively. We see that the modes of family member PROGSURF use all listed initial conditions (altogether 7) and all atmospheric forcing data excepted T_S (altogether 5), whereas the Pm-PTSURF mode needs the smallest number of initial (4 in all) and forcing data (4 in all).

Table 2a. SURFMOD family members and modes and their initial conditions

Initial conditions of SURFMOD								
Family member	Mode	T_{vg}	T_{dg}	M_v	θ_{l1}	θ_{s1}	θ_2	θ_3
PROGSURF	Psi1	used	used	used	used	used	used	used
	Psi2	used	used	used	used	used	used	used
	Theta	used	used	used	used	used	used	used
	Combin.	used	used	used	used	used	used	used
PMSURF	Psi1	not used	not used	used	used	not used	used	used
	Theta	not used	not used	used	used	not used	used	used
PTSURF	Prog	used	used	used	used	used	used	used
	Pm	not used	not used	used	used	not used	used	used

Symbols: T_{vg} – vegetation-ground temperature, T_{dg} – deep-ground temperature, M_v – water stored in the vegetation layer, θ_{l1} – liquid moisture content in the 1st soil layer, θ_{s1} – solid moisture content in the 1st soil layer, θ_2 – moisture content in the 2nd soil layer and θ_3 – moisture content in the 3rd soil layer

Table 2b. SURFMOD family members and modes and their atmospheric forcing data

Atmospheric forcing data of SURFMOD							
Family member	Mode	T_r	e_r	V_r	S	R_a	T_S
PROGSURF	Psi1	used	used	used	used	used	not used
	Psi2	used	used	used	used	used	not used
	Theta	used	used	used	used	used	not used
	Combin.	used	used	used	used	used	not used
PMSURF	Psi1	used	used	used	used	used	used
	Theta	used	used	used	used	used	used
PTSURF	Prog	used	not used	used	used	used	not used
	Pm	used	not used	not used	used	used	used

Symbols: T_r – air temperature, e_r – air humidity, V_r – wind speed, S – solar radiation, R_a – downward atmospheric radiation and T_S – ground surface temperature

SURFMOD's basic features and the main differences between its family members and modes are comparatively presented in the form of tables. The differences are separately presented for prognostic equations, heat fluxes and the relevant parameters in *Table 3, 4* and *5*, respectively. There are no differences in the prediction of soil moisture and vegetation water storage. All modes apply the Richards' equation for soil moisture prediction (*Ács* and

Table 3. SURFMOD family members and modes and their prognostic equations

Prognostic equations of SURFMOD				
Family member	Mode	Water storage on vegetation	Temperature	Soil moisture
PROGSURF	Psi1	budget equation	force-restore method	Richard's equation
	Psi2	budget equation	force-restore method	Richard's equation
	Theta	budget equation	force-restore method	Richard's equation
	Combin.	budget equation	force-restore method	Richard's equation
PMSURF	Ps1	budget equation	–	Richard's equation
	Theta	budget equation	–	Richard's equation
PTSURF	Prog	budget equation	force-restore method	Richard's equation
	Pm	budget equation	–	Richard's equation

Hantel, 1998b) and the mass budget equation for water storage in vegetation layer. Temperature is predicted by the force-restore method or not predicted at all. Then the Penman-Monteith concept is applied where there is no parameterization of soil water freezing or melting.

Table 4. SURFMOD family members and modes and their heat flux parameterizations

SURFMOD heat fluxes				
Family member	Mode	Latent heat flux	Sensible heat flux	Ground heat flux
PROGSURF	Psi1	aerodynamic formula	aerodynamic formula	conduction equation
	Psi2	aerodynamic formula	aerodynamic formula	conduction equation
	Theta	aerodynamic formula	aerodynamic formula	conduction equation
	Combi-nation	Penman-Monteith equation	aerodynamic formula	conduction equation
PMSURF	Ps1	Penman-Monteith equation	residual from energy balance equation	percentage of net radiation
	Theta	Penman-Monteith equation	residual from energy balance equation	percentage of net radiation
PTSURF	Prog	Priestley-Taylor equation	aerodynamic formula	conduction equation
	Pm	Priestley-Taylor equation	residual from energy balance equation	percentage of net radiation

There are also great differences in the heat flux parameterizations (Table 4). Latent heat flux is parameterized either by the aerodynamic formula or by the Penman-Monteith formula or by the Priestley-Taylor formula. Sensible heat flux is calculated either by the aerodynamic formula or as a residiual term from the energy balance equation (*Ács* and *Hantel*, 1999). Ground heat flux is calculated either at 10 cm depth G_1 or at the ground surface G_0. G_1 is parameterized in conjunction with the force-restore method by a heat conduction equation while G_0 is estimated as the percentage of net radiation.

Table 5. SURFMOD family members and modes and their parameters representing soil and atmospheric state

SURFMOD parameters representing soil and atmospheric state				
Family member	Mode	Aerodynamic transfer	Available soil moisture	Atmospheric demand
PROGSURF	Psi1	resistance concept	F_{ma} is parameterized by leaf water potential	$0 < F_{ad} \leq 1$
	Psi2	resistance concept	F_{ma} is parameterized by leaf water potential	$F_{ad} \equiv 1$
	Theta	resistance concept	F_{ma} is parameterized by soil moisture	$0 < F_{ad} \leq 1$
	Combi-nation	resistance concept	F_{ma} is parameterized by leaf water potential	$0 < F_{ad} \leq 1$
PMSURF	Ps1	resistance concept	F_{ma} is parameterized by leaf water potential	$0 < F_{ad} \leq 1$
	Theta	resistance concept	F_{ma} is parameterized by soil moisture	$0 < F_{ad} \leq 1$
PTSURF	Prog	resistance concept	moisture availability function β	$E(\theta_S)$
	Pm	–	moisture availability function β	$E(\theta_S)$

Symbols: F_{ad} – atmospheric demand function in the canopy resistance parameterization, F_{ma} – moisture availability function in the canopy resistance parameterization and $E(\theta)_S$ – potential evapotranspiration

SURFMOD family members and modes differ also in the parameterizations of some relevant parameters. The applied parameterizations for aerodynamic transfer, available soil moisture and atmospheric demand are reviewed in Table 5. The aerodynamic transfer is parameterized using the resistance concept with

the Monin-Obukhov similarity theory or not parameterized at all. Then the Penman-Monteith concept with the Priestley-Taylor formula is applied. The effect of available soil moisture upon transpiration is expressed either via stress function F_{ma} or by soil moisture availability function β. F_{ma} can be parameterized by both the soil moisture content and the leaf water potential (*Ács* and *Hantel,* 1998b). The atmospheric demand is parameterized via stress function F_{ad} or via estimation of potential evapotranspiration. F_{ad} can vary between 0 and 1 or it is equal to 1 (*Ács* and *Hantel,* 1998a). In the Priestley-Taylor formula applications the atmospheric demand is parameterized estimating potential evapotranspiration.

Inspecting SURFMOD family members and modes, it is obvious that the most complex SURFMOD mode is the Psi1-PROGSURF while the simpliest mode is the Pm-PTSURF. In the following these two modes will be comparatively presented with more details.

2.1 Prognostic equations

The main difference between Psi1-PROGSURF and Pm-PTSURF is in the application of temperature prediction equations. In the following this aspect will be presented with more attention.

- **Psi1-PROGSURF:** The temperature prediction of vegetation-ground and deep-ground layers is made by using the force restore method (*Bhumralkar,* 1975).

$$C_B \cdot \frac{\partial T_{vg}}{\partial t} = F(T_{vg}, \theta_{l1}, \theta_{s1}), \tag{1}$$

$$\frac{\partial T_{dg}}{\partial t} = \frac{1}{\tau} \cdot (T_{vg} - T_{dg}), \tag{2}$$

where

$$C_B = veg \cdot C_v + (1 - veg) \cdot C_b, \tag{3}$$

$$C_b = 10\ \text{cm} \cdot C + \left(\frac{\lambda \cdot C}{2\,\omega}\right)^{1/2}, \tag{4}$$

$$C = (1 - \theta_{S1}) \cdot C_m + \theta_{l1} \cdot C_l + \theta_{s1} \cdot C_s, \tag{5}$$

$$F(T_{vg}, \theta_{l1}, \theta_{s1}) = (R + H + L \cdot E - G_1) \cdot \delta\,(T_{vg}, \theta_{l1}, \theta_{s1}). \tag{6}$$

The parameter C_B is the bulk heat capacity of the vegetation-ground system (J m^{-2} K^{-1}), C_b is the bulk heat capacity of the upper 10 cm of bare soil (J m^{-2} K^{-1}), C_v is the vegetation heat capacity (J m^{-2} K^{-1}), C is the volumetric heat capacity of the soil surface layer (J m^{-3} K^{-1}), λ is the thermal conductivity of the soil surface layer (W m^{-1} K^{-1}), ω is the angular velocity of the rotation of the earth (s^{-1}), C_m is the volumetric heat capacity of solid soil particles (J m^{-3} K^{-1}), C_l is the volumetric heat capacity of water (J m^{-3} K^{-1}), C_s is the volumetric heat capacity of ice (J m^{-3} K^{-1}) and τ is the length of the day (s). With the step function δ the model switches between unfrozen, partly frozen and totally frozen soil as follows:

$$\delta\,(T_{vg}, \theta_{l1}, \theta_{s1}) = \begin{cases} 1 & \text{for } T_{vg} > T_{fr},\ \theta_{l1} \geq 0,\ \theta_{s1} = 0 \\ 0 & \text{for } T_{vg} = T_{fr},\ \theta_{l1} > 0,\ \theta_{s1} > 0 \\ 1 & \text{for } T_{vg} < T_{fr},\ \theta_{l1} = 0,\ \theta_{s1} \geq 0. \end{cases} \tag{7}$$

δ regulates the temperature prediction of the vegetation-ground system. During soil freezing/melting processes, T_{vg} is equal to the freezing temperature T_{fr} and temperature prediction is switched off, represented by $F(T_{vg}, \theta_{l1}, \theta_{s1}) \equiv 0$. In the absence of soil freezing/melting processes the temperature prediction of the vegetation-ground system is switched on. The energy budget function $F(T_{vg}, \theta_{l1}, \theta_{s1})$ refers to the vegetation-ground layer. R, H and $L \cdot E$ are net radiation, sensible and latent heat fluxes across the surface (W m^{-2}), G_1 is the soil heat flux across the bottom of the 1st soil layer (W m^{-2}) and L is the latent heat of vaporization (J kg^{-1}).

- **Pm-PTSURF:** Pm-PTSURF does not apply temperature prediction equations at all. Consequently there is no representation of soil water freezing/melting processes.

2.2 Radiation

The are no differences in the parameterization of radiation between the two modes.

2.3 Turbulent heat fluxes

The turbulent heat flux parameterizations are completely different in Psi1-PROGSURF and Pm-PTSURF. They are as follows:

- **Psi1-PROGSURF:** The latent heat flux is parameterized by

$$L \cdot E^j = -\frac{\rho\, c_p}{\gamma} \frac{f^j \cdot e_S(T_{vg}) - e_r}{r_a^j + r^j}, \tag{8}$$

where ϱ is the air density, c_p is the specific heat of air at constant pressure, γ is the psychrometric constant, $e_S(T_{vg})$ is the saturation vapor pressure at T_{vg}, e_r is the vapor pressure at the reference level and r_a^j is the aerodynamic resistance. The superscript j refers to the domains of vegetation (j=v) with relative coverage *veg*, and of bare soil (j=b) with coverage 1-*veg*. For vegetation we additionally distinguish between wet (j=vw) and dry (j=vd). In both cases we put

$$f^{vw} = f^{vd} = 1. \tag{9}$$

The wet/dry distinction applies only to the surface resistance r^j.

The sensible heat flux is parameterized as

$$H^j = -\rho\, c_p \frac{T_{vg} - T_r}{r_a^j}, \tag{10}$$

where T_r is the reference temperature.

The horizontal mean values of turbulent fluxes are estimated by

$$L \cdot E \quad \text{with} \quad E = veg \cdot E^v + (1 - veg) \cdot E^b \tag{11}$$

and

$$H = veg \cdot H^v + (1 - veg) \cdot H^b. \tag{12}$$

- **Pm-PTSURF:** The latent heat flux is expressed using the soil moisture availability concept, that is

$$L \cdot E^j = \beta^j \cdot L \cdot E_p^j, \tag{13}$$

where E and E_p is the actual and potential evapotranspiration and β is the moisture availability function. As above, the index j represents the surface type. The potential evapotranspiration rate $L \cdot E_p^j$ is parameterized using the Priestley-Taylor formula (*Priestley* and *Taylor*, 1972), that is

$$L \cdot E_p^j = \alpha \cdot \frac{\Delta}{\Delta + \gamma} \cdot A^j, \tag{14}$$

where α =1.26 is the Priestley-Taylor coefficient, Δ is the slope of saturated

vapor pressure curve at T_r, A^j is the available energy of surface. For bare soil $A^j = R^j - G^j$ but for vegetation $A^j = R^j$. R^j is the net radiation flux while G^j is the ground surface heat flux.

The sensible heat flux is estimated as residual,

$$H^j = A^j - L \cdot E^j. \tag{15}$$

The horizontal mean values of turbulent fluxes are obtained by Eq. (11) and Eq. (12).

2.4 Ground heat flux

There is a great difference in the ground heat flux parameterization between Psi1-PROGSURF and Pm-PTSURF. The parameterizations used are briefly considered below.

- **Psi1-PROGSURF:** The ground heat flux at 10 cm depth is estimated in conjunction with force-restore method as

$$G_1 = \left(\frac{\omega \cdot C_B \cdot \lambda}{2} \right)^{1/2} \cdot (T_{vg} - T_{dg}). \tag{16}$$

G_1 represents the horizontal mean value.

- **Pm-PTSURF:** The ground heat flux at earth surface is parameterized as the percentage of net radiation.

$$G_0^b = 0.15 \cdot R^b. \tag{17}$$

Under vegetation canopy it can be neglegted, therefore

$$G_0^v = 0. \tag{18}$$

The horizontal mean of G_0 is calculated as in Eq. (11) or Eq. (12).

2.5 Water fluxes

There are no differences in the parameterization of water transfer in the soil and canopy layer between the two modes. The set of equations applied are presented in *Ács* and *Hantel* (1998a). The only difference between the two modes is in the parameterization of evapotranspiration. This is presented in section 2.3.

2.6 Aerodynamic transfer

- **Psi1-PROGSURF:** The aerodynamic transfer is parameterized via the resistance concept using the Monin-Obukhov similarity theory taking into account the atmospheric stability. The aerodynamic resistance is split into laminar and turbulent terms distinguishing transports between momentum and heat/moisture. The resistances are separately calculated above vegetated and bare soil surfaces.

- **Pm-PTSURF:** There is no aerodynamic transfer parameterization since the turbulent fluxes do not depend upon aerodynamic transfer.

2.7 Available soil moisture

There is a great difference in the parameterization of available soil moisture between Psi1-PROGSURF and Pm-PTSURF. The parameterizations are considered separately for vegetation and bare soil surafce.

2.7.1 Vegetation

- **Psi1-PROGSURF:** The soil moisture available for transpiration is parameterized using the resistance concept. The well known *Jarvis* (1976) formula is applied:

$$r^{vd} = \frac{r_{stmin} \cdot F_{ad}}{LAI \cdot GLF \cdot F_{ma}}, \tag{19}$$

where r^{vd} is the canopy resistance, r_{stmin} is the minimum stomatal resistance at optimum environmental conditions. *LAI* is the leaf area index, *GLF* is the green leaf fraction; it expresses the fraction of live leaves ranging between 0 and 1. F_{ad} and F_{ma} represent the atmospheric demand and moisture availability effect upon stomatal functioning, respectively; they range between 0 and 1.

- **Pm-PTSURF:** The soil moisture/transpiration dependence is parameterized via soil moisture availability function β^v. It is expressed as

$$\beta^v = \begin{cases} 1 & \text{for } \theta_{rz} \geq \theta_c \\ \dfrac{\theta_{rz}}{\theta_c} & \text{for } \theta_{rz} < \theta_c, \end{cases} \tag{20}$$

where θ_{rz} is the soil moisture content in the root zone and θ_c is the critical soil moisture content. It is parameterized by

$$\theta_c = 0.75 \cdot \theta_f, \tag{21}$$

where θ_f is the moisture content at field capacity.

2.7.2 Bare soil

- *Psi1-PROGSURF:* The soil moisture available for evaporation is also parameterized via the resistance concept. The soil surface resistance r^b is estimated by *Sun*'s (1982) empirical formula:

$$r^b = c_1 + c_2 \cdot \left(\frac{\theta_{S1}}{\theta_1} \right)^{c_3}, \tag{22}$$

where θ_1 and θ_{S1} is the actual and saturated soil moisture content in the 1st soil layer. c_1, c_2 and c_3 are empirical constants (for constants see Table 2 in *Ács* and *Hantel*, 1998a).

- *Pm-PTSURF:* The soil moisture availability function for bare soil surface β^b is analogously parameterized to β^v. It is expressed by

$$\beta^b = \begin{cases} 1 & \text{for } \theta_1 \geq \theta_c \\ \dfrac{\theta_1}{\theta_c} & \text{for } \theta_1 < \theta_c . \end{cases} \tag{23}$$

2.8 Soil water freezing or melting

- **Psi1-PROGSURF:** There is soil water freezing or melting in the vegetation-ground layer. The parameterization applied is shortly described in *Ács* and *Hantel* (1998a).

- *Pm-PTSURF:* Soil water freezing or melting processes can not be represented since there is no T_{vg}-temperature prediction.

3. Validation of the models

The model family SURFMOD has been extensively tested in off-line mode using the 1987 data from Cabauw, The Netherlands. The Cabauw data set is a PILPS data set. Its complete description is given in Beljaars and Bosveld (1997). In the numerical experiments SURFMOD was always initialized as all PILPS participating models by saturating all liquid water stores. The variable and constant land-surface parameters are specified according to the specifications used in PILPS phase 2a experiment (see Table A2, A3 and A4 in *Chen et al.*, 1997 or Table 1 and 2 in *Ács* and *Hantel*, 1998a).

The model validation is performed by comparing simulated and observed surface fluxes. In the following the annual mean characteristics, the seasonal changes and the instantaneous values obtained in the IOP (intensive observation period) of the most important turbulent heat and water balance components are shortly described. At the end we are going to try to explain the results, that is the behaviour of SURFMOD modes.

3.1 Annual mean characteristics

The spinup time of both SURFMOD modes is 2 years. The annual mean sensible and latent heat fluxes of Psi1-PROGSURF and Pm-PTSURF together with other PILPS results are presented in *Fig. 1*. The sensible heat flux of Pm-PTSURF is -7.4 W m^{-2}, the latent heat flux is -34.7 W m^{-2}. The point is exactly located on the net radiation line since the measured net radiation is used as input. The corresponding point for Psi1-PROGSURF is not closer to the observation but the somewhat under net radiation line. This deviation from net radiation line is caused by application of force-restore method (*Ács* and *Hantel*, 1999).

The annual runoff versus evapotranspiration is given in *Fig. 2*. There is only a minor difference between the results obtained by Psi1-PROGSURF (E = -435 mm yr^{-1} and R = 337 mm yr^{-1}) and Pm-PTSURF (E = -440 mm yr^{-1} and R = 332 mm yr^{-1}). Pm-PTSURF's result is slightly closer to the observation than the Psi1-PROGSURF's result.

3.2 Seasonal variations

The seasonal change of sensible heat flux and evapotranspiration is presented in *Figs. 3* and *4*, respectively. According to the convention applied all vertical fluxes are positive if directed downwards. Inspecting Fig. 3 we see that the difference between the simulation results is small in summer but large in October, November and December. The results obtained by Psi1-PROGSURF are closer to the observations with respect to Pm-PTSURF's results. This is especially obvious in autumn.

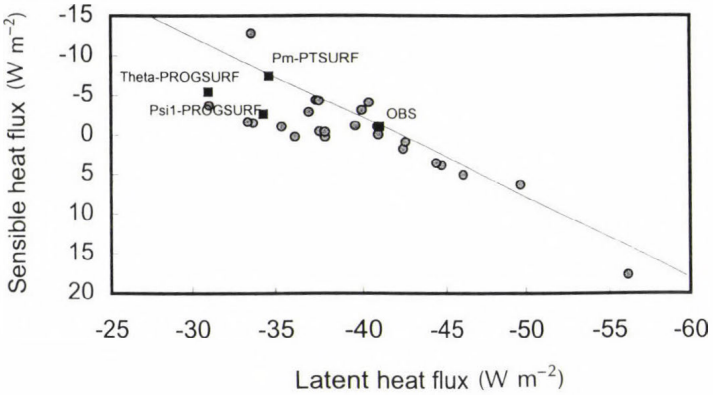

Fig. 1. Annually averaged sensible versus latent heat fluxes estimated by modes Pm-PTSURF, Psi1-PROGSURF and Theta-PROGSURF (thick symbols) along with the equivalent PILPS phase 2a results (thin dots; for details see Fig. 5 in *Chen et al.*, 1997). The SURFMOD modes are characterised in Table 1; OBS = observed value.

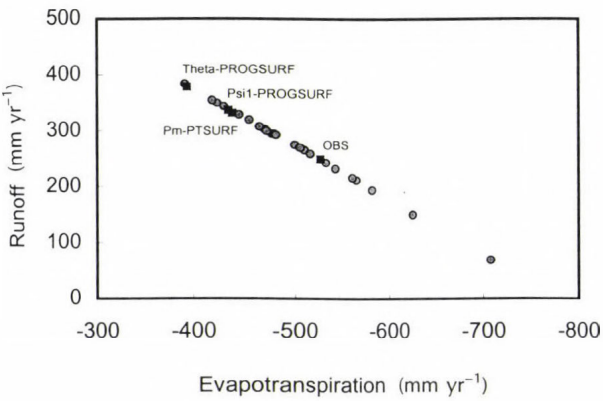

Fig. 2. As Fig. 1 but for runoff versus evapotranspiration (compare with Fig. 10 in *Chen et al.*, 1997).

Fig. 4 presents the simulated and observed evapotranspiration. The main characteristics can be summarized as follows: Pm-PTSURF yields better results than Psi1-PROGSURF in February, March, April and May but Psi1-PROGSURF is more superior with respect to Pm-PTSURF in October, November and December. In summer months the simulation results do not show any observable tendency.

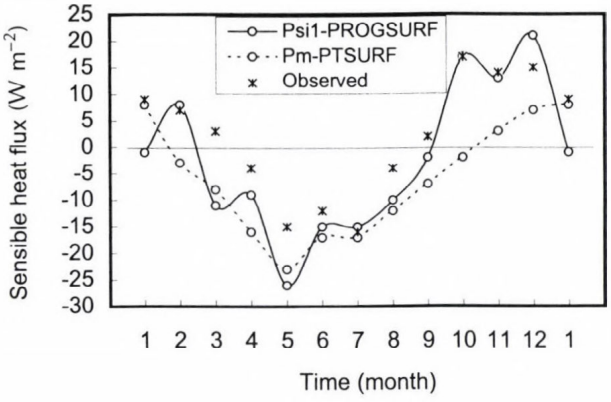

Fig. 3. Annual course of sensible heat flux simulated by Psi1-PROGSURF and Pm-PTSURF.

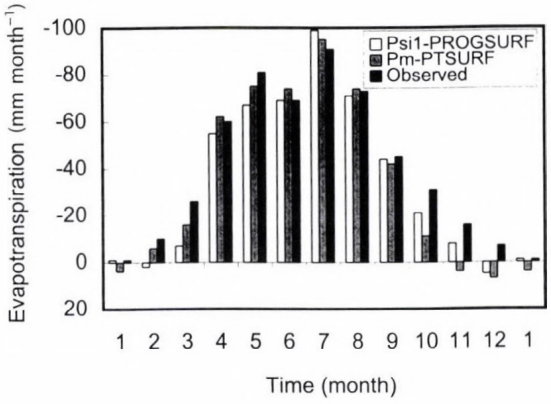

Fig. 4. Annual course of evapotranspiration simulated by Psi1-PROGSURF and Pm-PTSURF.

3.3 Turbulent fluxes in the intensive observation period

Instantaneous values of turbulent heat fluxes have been measured in the intensive observation period between September 10–19, 1987. The comparison of simulated and observed latent heat fluxes for Psi1-PROGSURF and Pm-PTSURF is presented in *Figs. 5* and *6*, respectively. The results obtained are suitable: The correlation coefficients obtained are between 0.8 and 0.9; the slope of regression lines obtained by Psi1-PROGSURF and Pm-PTSURF are 0.97 and 1.55, respectively. The comparison of simulated and observed sensible

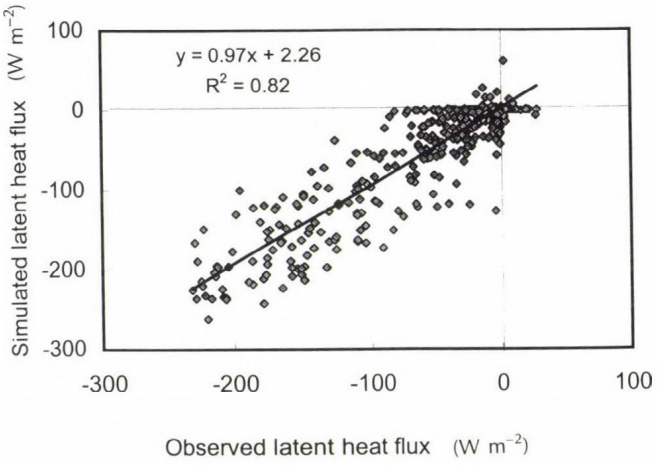

Fig. 5. Psi1-PROGSURF-simulated versus observed latent heat flux in the IOP (from day 253 to day 262). Thick line: regression.

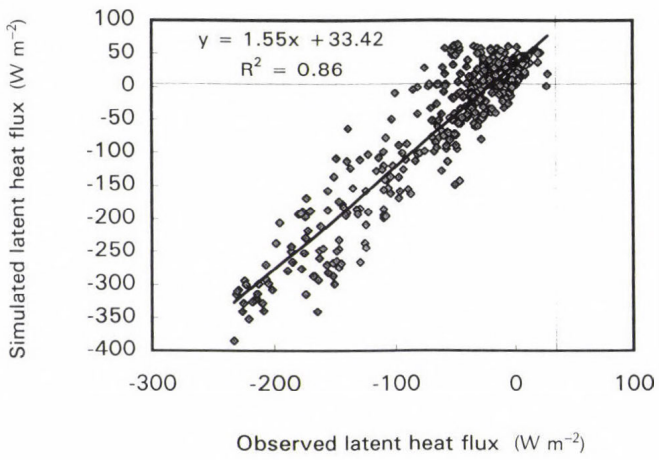

Fig. 6. Pm-PTSURF-simulated versus observed latent heat flux in the IOP (from day 253 to day 262). Thick line: regression.

heat fluxes for Psi1-PROGSURF and Pm-PTSURF is presented in *Figs. 7* and *8*, respectively. The correlation coefficients obtained are less than for the latent heat flux but still above 0.69. The slope of the regression lines deviates from 1; it amounts 0.78 for Psi1-PROGSURF and 0.47 for Pm-PTSURF.

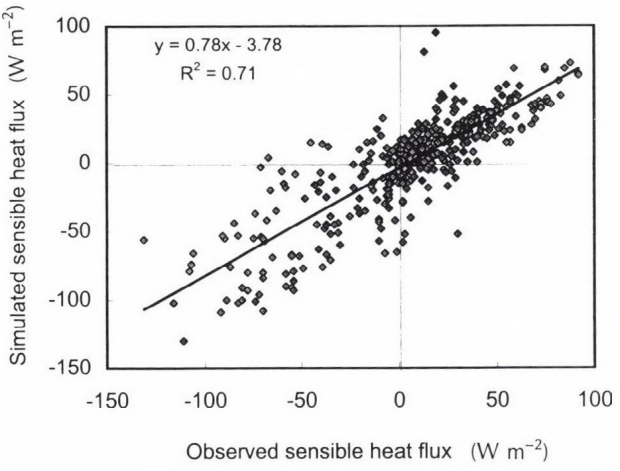

Fig. 7. Psi1-PROGSURF-simulated versus observed sensible heat flux in the IOP (from day 253 to day 262). Thick line: regression.

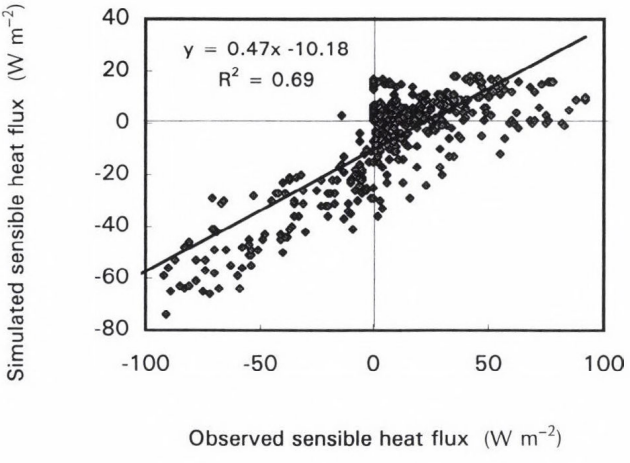

Fig. 8. Pm-PTSURF-simulated versus observed sensible heat flux in the IOP (from day 253 to day 262). Thick line: regression.

3.3.1 Analyses of the results

The results obtained by Psi1-PROGSURF and Pm-PTSURF can be explained by analysing simultaneously both the seasonal change of root-zone soil water

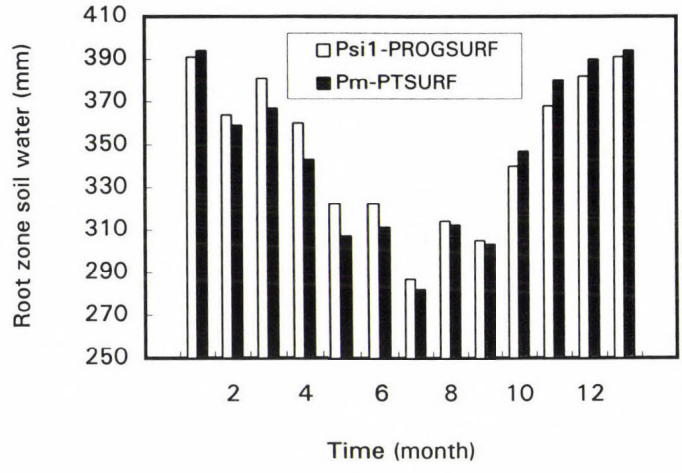

Fig. 9. Annual course of root-zone soil water simulated by Psi1-PROGSURF and Pm-PTSURF.

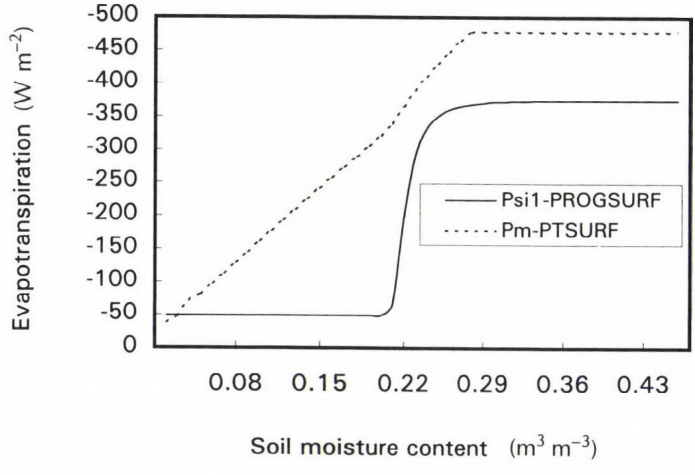

Fig. 10. Evapotranspiration versus root-zone soil moisture simulated by Psi1-PROGSURF and Pm-PTSURF. The soil/vegetation parameter refers to the Cabauw site. The atmospheric boundary conditions used are as follows: the global radiation is 800 W m^{-2}, air temperature, vapor pressure and wind velocity at the reference level is 25.8°C, 18 hPa and 6.0 m s^{-1}, respectively, and there is no precipitation.

and the evapotranspiration/soil moisture content relationship $E(\theta)$. The annual course of root-zone soil water for both SURFMOD modes is presented in Fig. 9, while the $E(\theta)$ relationships are drawn in *Fig. 10*. $E(\theta)$ curves need special

attention. Both $E(\theta)$ curves are determined by the slope $S = \partial E(\theta)/\partial\theta$ in the transition region and the saturation value $E(\theta_S)$. Note that for Pm-PTSURF $E(\theta_S) = E_p$. Evidently, for low values of θ (dry surface), the evapotranspiration $E(\theta)$ is independent of both S and $E(\theta_S)$. For extremely high values of θ (well-watered surface) it is only dependent upon $E(\theta_S)$. In the transition zone both parameters $E(\theta_S)$ and S become active.

Inspecting Fig. 10 we see that there is a drastic deviation between the $E(\theta)$ curves obtained by Psi1-PROGSURF and Pm-PTSURF. The deviations are enormously great for low θ values up to about $\theta = 0.22$ m^3 m^{-3}. The deviations are constant and considerably less for high θ values that is in the saturation zone of $E(\theta)$ curves. At the same time Fig. 9 shows that the soil moisture in summer for the Cabauw data is between about 0.28 and 0.34 m^3 m^{-3}; i.e., it is located even in the saturation zone of $E(\theta)$ curves. Note the difference between root zone soil *moisture* (abscissa of Fig. 10) and root zone soil *water* (ordinate of Fig. 9) although both quantities are proportional. Thus, the evapotranspiration for the Cabauw site is controlled by the parameter $E(\theta_S)$; the parameter S is of no importance. Since there is an acceptable deviation between the parameter $E(\theta_S)$ obtained by Psi1-PROGSURF and Pm-PTSURF, the deviations between their simulation results are also not great.

4. Conclusion

An overview of the land-surface model family SURFMOD is given. We paid more attention to the comparison of the most complex Psi1-PROGSURF and the simpliest Pm-PTSURF modes. Pm-PTSURF deviates from the Psi1-PROGSURF as follows:

- air humidity is not used but net radiation or surface temperature is used as input (see Table 2b),
- ground heat flux at surface is calculated via net radiation (see Table 4),
- latent heat flux is parameterized via the Priestley-Taylor formula which implies no leaf water potential calculation (see Table 4),
- sensible heat flux is estimated as the residiual from the energy balance equation (see Table 4) and
- the applied method for latent and sensible heat flux parameterization implies that there is no need for aerodynamic resistance calculation (see Table 5) as well as that in winter no snow and/or soil freezing/melting processes can be represented (see Table 2a).

Summarizing the deviations we can say that Pm-PTSURF is not only simple with respect to Psi1-PROGSURF but also it is extremely simple with respect to other biophysical models (*Shao* and *Henderson-Sellers*, 1996).

Psi1-PROGSURF and Pm-PTSURF has been compared in off-line mode for the Cabauw data set, using the same specifications that have been applied in the PILPS campaign (*Chen et al.*, 1997). The models reproduces satisfactorily the observed annual mean values, the seasonal changes and the instantaneous values of turbulent and water fluxes. For example, the annual mean values of evapotranspiration and runoff obtained by Pm-PTSURF are -440 and 332 mm, respectively. This result proves that Pm-PTSURF can capture—in spite of its extreme simplicity—those relevant phenomenons which determine the Cabauw site: the potential evapotranspiration governed by atmospheric conditions during almost the full year. Moreover it yields better results in terms of turbulent and water fluxes with respect to some much more complex SURFMOD modes as for example Theta-PROGSURF (see Fig. 1 and 2). This numerical experiment proves that the extremely simple models as Pm-PTSURF can also remarkably reproduce the observations. At the end, we have shown the main reason why the simulation results of Psi1-PROGSURF and Pm-PTSURF do not enormously deviate.

Further developments of the model family SURFMOD are in preparation. SURFMOD presently serves as a substitute for observed fluxes of latent and sensible heat for the software DIAMOD (*Hantel et al.*, 1993; *Haimberger et al.*, 1995) and also as an effective tool in performing comparative studies.

Acknowledgements—The authors wish to thank the *Österreichische Akademie der Wissenschaften* within the National Austrian Committee for the IGBP. We thank *Dr. L. Haimberger* for the helpful discussions and help in data transfer processing. The technical help provided by *Mr. Z. Barcza* has been very constructive and it is highly appreciated.

References

Ács, F., Mihailovic, D.T. and *Rajkovic, B.*, 1991: A coupled soil moisture and surface temperature prediction model. *J. Appl. Meteor. 30*, 812-822.

Ács, F., 1994: A coupled soil-vegetation scheme: Description, parameters, validation, and sensitivity studies. *J. Appl. Meteor. 33*, 268-284.

Ács, F., 1995: Simple surface flux model for use within diagnostic atmospheric models. *Proc. of the EGS XX General Assembly* (Supplements Issue of Annales Geophysicae, Part II., Supplement II to Volume 13), C470, Hamburg, 3-7 April.

Ács, F., Dorninger, M. and *Hantel, M.*, 1996: The Surface Flux Model SURFMOD. User Manual. *Internal Report of the Institute for Meteorology and Geophysics, University of Vienna.*

Ács, F. and *Hantel, M.*, 1998a: The Land-Surface Flux Model PROGSURF. *Global Planet. Change 19*, 19-34.

Ács, F. and *Hantel, M.*, 1998b: The Land-Surface Hydrology Parameterization in PROGSURF: Formulation and Test Results with Cabauw Data Set. *Időjárás 102*, 109-127.

Ács, F., Dorninger, M. and *Hantel, M.*, 1998a: The Land-Surface Model PROGSURF. User Manual. *Internal Report of the Institute for Meteorology and Geophysics, University of Vienna.*

Ács, F., Dorninger, M. and *Hantel, M.*, 1998b: The Land-Surface Model PMSURF. User Manual. *Internal Report of the Institute for Meteorology and Geophysics, University of Vienna.*

Ács, F. and *Hantel, M.*, 1999: The Penman-Monteith concept based land-surface model PMSURF. *Időjárás 103*, 19-36.

Ács, F., Hantel, M. and *Unegg, J.*, 2000: The Budapest-Vienna Land-Surface Model Family SURFMOD. *Internal Report of the Institute for Meteorology and Geophysics, University of Vienna.*

Bhumralkar, C.M., 1975: Numerical experiments on the computation of ground surface temperature in an atmospheric general circulation model. *J. Appl. Meteor. 14,* 1246-1258.

Beljaars, A.C.M. and *Bosveld, F.C.*, 1997: Cabauw data for the validation of land surface parameterization schemes. *J. Climate 10*, 1172-1194.

Chen, T.H., Henderson-Sellers, A., Milly, P.C.D., Pitman, A.J., Beljaars, A.C.M., Polcher, J., Abramopoulos, F., Boone, A., Chang, S., Chen, F., Dai, Y., Desborough, C.E., Dickinson, R.E., Dumenil, L., Ek, M., Garratt, J.R., Gedney, N., Gusev, Y.M., Kim, J., Koster, R., Kowalczyk, E.A., Laval, K., Lean, J., Lettenmaier, D., Liang, X., Mahfouf, J.-F., Mengelkamp, H.-T., Mitchell, K., Nasonova, O.N., Noilhan, J., Robock, A., Rosenzweig, C., Schaake, J., Schlosser, C.A., Schulz, J.-P., Shao, Y., Shmakin, A.B., Verseghy, D.L., Wetzel, P., Wood, E.F., Xue, Y., Yang, Z.-L. and *Zeng, Q.*, 1997: Cabauw experimental results from the project for intercomparison of land-surface parameterization schemes. *J. Climate 10,* 1194-1216.

Dolman, A.J., 1993: A multiple-source land surface energy balance model for use in general circulation models. *Agric. Forest Meteorol. 65,* 21-45.

Haimberger, L., Hantel, M. and *Dorninger, M.*, 1995: A thermodynamic model for the atmosphere. Part III: DIAMOD with orography and improved error model. *Meteorol. Zeitschrift., N.F. 4*, 162-182.

Hantel, M., Ehrendorfer, M. and *Haimberger, L.*, 1993: A thermodynamic diagnostic model for the atmosphere. Part II: The general theory and its consequences. *Meteorol. Zeitschrift, N.F. 1*, 87-121.

Jarvis, P.G., 1976: The interpretation of the variations in leaf water potential and stomatal conductance found in canopies in the field. *Philos. Trans. Roy. Soc. London*, Ser. B., 273, 593-610.

Monteith, J.L., 1965: Evaporation and Environment. In *The State and Movement of Water in Living Organisms* (ed.: *G. Fogg*). *Proc. 19th Symp. Soc. Exp. Biol.*, Cambridge, Cambridge University Press, 205-236.

Monteith, J., 1995: Accomodation between transpiring vegetation and the convective boundary layer. *J. Hydrol. 166*, 536-550.

Priestley, C.H.B. and *Taylor, R.J.*, 1972: On the assessment of surface heat flux and evaporation using large-scale parameters. *Mon. Wea. Rev. 100*, 81-92.

Shao, Y. and *Henderson-Sellers, A.*, 1996: Validation of soil moisture simulation in landsurface parameterization schemes with HAPEX data. *Global Planet. Change 13,* 11-46.

Sun, S.F., 1982: Moisture and heat transport in a soil layer forced by atmospheric conditions. *M.S. Thesis, Dept. of Civil Engineering, University of Connecticut.*

IDŐJÁRÁS

Quarterly Journal of the Hungarian Meteorological Service
Vol. 104, No. 1, January–March 2000, pp. 43–51

A method to estimate temporal behavior of extreme quantiles

István Matyasovszky

Department of Meteorology, Eötvös Loránd University,
H-1117 Budapest, Pázmány Péter sétány 1/A; E-mail: matya@ludens.elte.hu

(Manuscript received 3 December 1999; in final form 8 January 2000)

Abstract—Quantiles at tails of a density function with infinite support are defined as extremes, and a method is presented to estimate their temporal variations. The procedure does not need any specifications on the probability distribution, the unique assumption is its smooth variation in time. As an illustration, the methodology is applied to daily maximum and minimum temperature time series in Hungary. The example demonstrates that extremes may exhibit considerably variations when conventional trend estimates do not show statistically significant changes.

Key-words: extremes, quantile, time dependent distribution, maximum and minimum temperatures.

1. Introduction

Detection and estimation of climatic changes in observed data series have a broad literature. Examinations are principally based on variations of mean, i.e., much of these works uses particular versions of trend models (*Zheng* and *Basher*, 1999). However, several other statistical properties may vary during a changing climate. For instance, long-term change of extremes is an especially important issue for its socio-economic impacts.

The term "extremes" can be defined by several ways. These include such as the average returning period of an occurrence arising with small probabilities, probability distribution of maximum or minimum of a variable during a specific period, number of exceedances of high or low thresholds, duration below or above these thresholds, and many other choices.

Theory of extremes is well-developed when data set in question consists of a sequence of identically and independently distributed variables (*Gumbel*, 1958; *Leadbetter et al.*, 1983; *Tiago de Oliveira*, 1986). Although asymptotic properties of extremes are valid for quite broad classes of dependent sequences,

the practical modeling encloses serious difficulties under temporal dependency. The most significant problem emerges when the underlying sequence does not consist of identically distributed variables, which is the case, for instance, in a changing climate. Therefore, our idea is to define the term "extreme" so simply that it can be handled for dependent and non-homogeneous time series.

Extreme event is now defined as an occurrence arising with small probabilities at tail(s) of a density function with infinite support of a given variable. Such an event can be specified with a high or low (or both) quantile(s), and the task is then to estimate its (their) temporal variation. This can be done when the probability distribution is smoothly varying in time.

Rest of the paper presents a methodology estimating time dependent quantiles. Then the procedure is applied to daily maximum and minimum temperature time series of four locations in Hungary. Finally, a section for discussion and conclusions is provided.

2. *Methodology*

Let $Y(t)$ be a continuous parameter stochastic process and denote the α quantile of the probability distribution of $Y(t)$ at time t as $q_\alpha(t)$, i.e., $q_\alpha(t)$ satisfies the equation

$$F_t(q_\alpha(t)) = \alpha, \tag{1}$$

where $F_t(y)$ is the probability distribution function of $Y(t)$ evaluated at $Y(t) = y$. An estimate $\hat{q}_\alpha(t)$ can be obtained from the observed pairs $(t_i, Y(t_i))$, $i = 1,\ldots,n$ by solving Eq. (1) after replacing F_t with an estimate $\hat{F}_t$. Here $Y(t_i)$ for any t_i is supposed to be independent from $Y(t_j)$, $t_j \neq t_i$. A choice of $\hat{F}_t$, which smooths over t, is

$$\hat{F}_t(y) = \sum_i K[(t_i - t)/b)\, I[Y(t_i) \leq y] / \sum_i K[(t_i - t)/b), \tag{2}$$

where K is a kernel function and I is the indicator function: $I[A] = 1$ if A is true, $I[A] = 0$ otherwise (*Magee et al.*, 1991). Eq. (2) is an extension for conditional distribution functions of the Parzen-Rosenblatt kernel density estimator (*Parzen*, 1962; *Rosenblatt*, 1956), or it can be considered as a specific case of the Nadaraya-Watson estimator (*Nadaraya*, 1964; *Watson*, 1964) when indicator series in Eq. (2) is regressed on t. The kernel function determines how to decrease the influence of an observation at t_i when moving off t, and the

bandwidth b determines the rate of this decrease. In order to have a "good" estimate Eq. (2), $F_t(y)$ is assumed to be slowly varying in time, which is now defined as $q_\alpha(t)$ has finite derivatives up to an order of $k>0$ for any $0<\alpha<1$.

K is generally defined on the interval [-1,1] and is called of order k if

$$\int_{-1}^{1} K(z) z^j dz = \begin{cases} 0, & 0<j<k, \\ 1, & j=0 \end{cases} \tag{3}$$

is satisfied. The parameter k coincides with the order of biasedness, i.e., using a kernel of order k, Eq. (2) delivers an estimate with an asymptotic bias proportional to kth derivative of F with respect to t. Since the probability distribution function is supposed to be smoothly varying in time, a small value for k can be chosen in Eq. (3). Supposing that F can be taken as a local linear function of time ($k = 2$), the optimal K in a sense defined in *Fan* (1992) is

$$K(z) = \frac{3}{4}(1 - z^2), \quad z \in [-1,1], \tag{4}$$

the so-called Epanechnikov kernel.

The bandwidth can be estimated by minimizing the cross-validated quantity

$$CV(b) = \sum_i L_\alpha(Y_i - \hat{q}_\alpha^{(i)}(t_i)), \tag{5}$$

where $L_\alpha(z) = |\alpha - I[z<0]| \cdot |z|$ is the loss function employed (*Koenker* and *Bassett*, 1978) and $\hat{q}_\alpha^{(i)}$ denotes the estimate of $q_\alpha(t_i)$ using bandwidth b with observation i omitted in Eq. (2).

3. Application

Daily maximum and minimum temperatures for four stations (Pécs, Szeged, Miskolc, Budapest KMI) for the period from 1901 to 1990 are examined with respect to their low and high time dependent quantiles. An analysis is performed with quantiles $\alpha = 0.01, 0.05, 0.10$, and with $1-\alpha$, respectively. Only the winter (December, January, February) and summer (June, July,

August) seasons are analyzed since the probability distribution function F changes considerably within the other two seasons.

As a first step the optimal bandwidth has to be estimated for both the maximum and minimum temperatures for every quantile and for both seasons. It is known that crossvalidated estimation of the bandwidth results in a degenerate choice of b = 0 when data series are autocorrelated (*Duin*, 1976) as it is the case for maximum or minimum temperatures. Therefore, quantity (5) has been modified such that $\hat{q}_\alpha^{(i)}$ denotes the estimate of $q_\alpha(t_i)$ using bandwidth b with observations omitted of a neighborhood of observation i. This neighborhood has been chosen 5 days since autocorrelations for lags larger than this value are quite small. An interesting experience of bandwidth estimation is that variability of optimal bandwidths corresponding to the two elements, seasons and quantiles, is surprisingly small. Therefore, in order to decrease the relatively large variance of bandwidth estimates, the mean of bandwidths has been calculated and used in Eq. (2). It is obtained to be 22 years. This simple operation results in a slightly biased estimation but with considerably smaller variance. Therefore, it can be expected that this unique value provides even better bandwidth estimates than the originally obtained particular ones.

Major results which are illustrated by quantiles 0.05 and 0.95 in *Figs. 1* and *2* can be summarized as follows. Generally, there are three phases of temperature changes. Considerably increasing or nearly constant values can be observed in the first part of the period, then a cooling starts from twenties-forties. Finally, a warming emerges again after fifties-seventies except for minimum temperature in summer. In winter, variation of low quantiles is remarkably larger than variation corresponding to high quantiles, which results in changes of variance, too. Summer has approximately same magnitudes of quantile variations. Direction of changes of low and high values is not strongly parallel producing further changes of variance. Behavior of Miskolc somewhat differs from other locations due to local climate effects.

An interesting question can be how these tendencies relate to changes in means. Therefore, a commonly used linear trend analysis was carried out for seasonal means of temperature data. *Tables 1* and *2* show the slope of trends indicating significant ones at a 5% probability level. To accept the hypothesis of no trend, the test statistic in absolute value should be smaller than 1.99. In spite of a general warming found in many time series (*Molnár* and *Mika*, 1997), there are fewer positive slopes than negative ones. Minimum temperatures do not exhibit any significant trends in winter, while the summer has strongly significant negative trends except for Budapest KMI where an almost significant (at a 5% level) increasing trend is detected. The individual behavior of Budapest KMI is probably due to a powerful urban effect. Maximum temperatures have no significant trends in both seasons with an exception of Miskolc in summer.

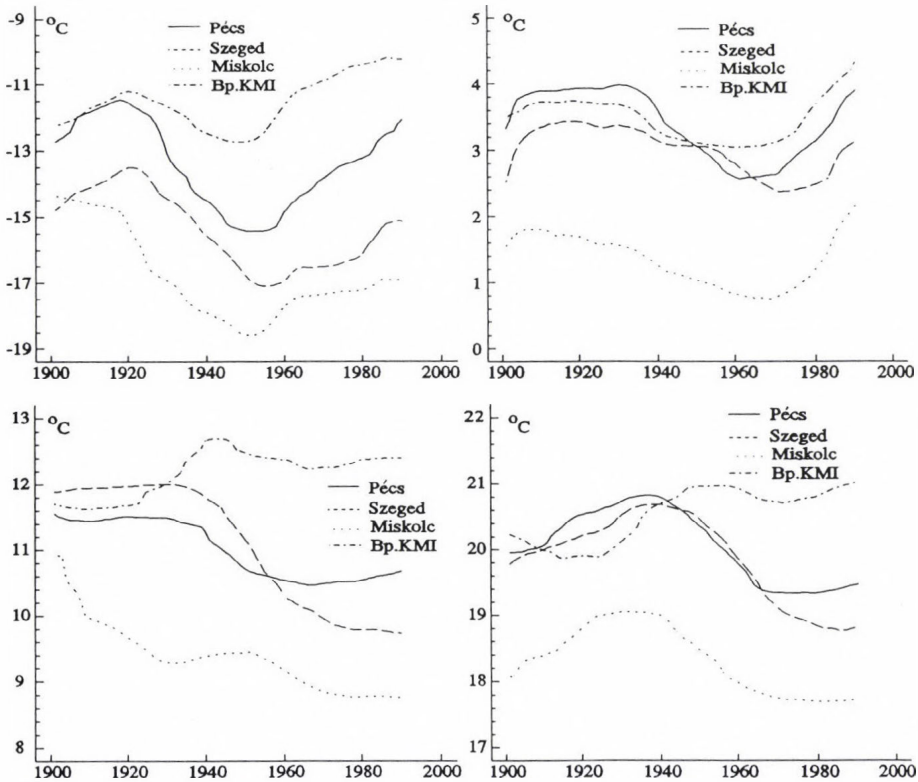

Fig. 1. Time dependent quantiles of daily minimum temperatures for $q = 0.05$ (left) and $q = 0.95$ (right) in winter (top) and summer (bottom).

There could be two reasons of these surprising findings. First, data series probably have considerable inhomogeneities, which, however, is beyond the scope of this study. Second reason is that the real trends are far from linearity; there can be warming and cooling phases during the entire period. In order to illustrate this fact *Fig. 3* shows seasonal mean temperature data and their corresponding linear trends for the following three cases: trend can be accepted as linear; trend is not linear; there is no trend. Seasonal mean of daily minimum temperature for Szeged in summer can be considered as an example for the first case. Fig. 1 and Fig. 3 show an intensive cooling from forties. However, behavior of both the 0.05 and 0.95 quantiles (Fig. 1) strengthens the visual observation for seasonal means that first part of the period does not suffer this cooling. Seasonal mean of daily maximum temperature for Pécs in summer, the second case mentioned above, makes the complex behavior of data more

clearer. No linear trend can be detected (Fig. 3), while the corresponding quantiles (Fig. 2) exhibit remarkable temporal changes. Looking at observed data in Fig. 3 at least one cooling interval in the middle of the period and two warming phases at boundaries can be recognized. This is clearly reproduced by time dependent quantiles (Fig. 2). Our last case is represented by seasonal mean of daily maximum temperature for Miskolc in winter. Here, seasonal means are scattered purely randomly around a line parallel with the axis of years (Fig. 3). Thus, the mean is certainly unchanged, but not so the quantiles. This can easily be understood because extremes are depend on the probability distribution and not on mean. For instance, supposing that daily maximum and minimum temperatures are distributed normally, the variance also has a key role in controlling extremes quantiles.

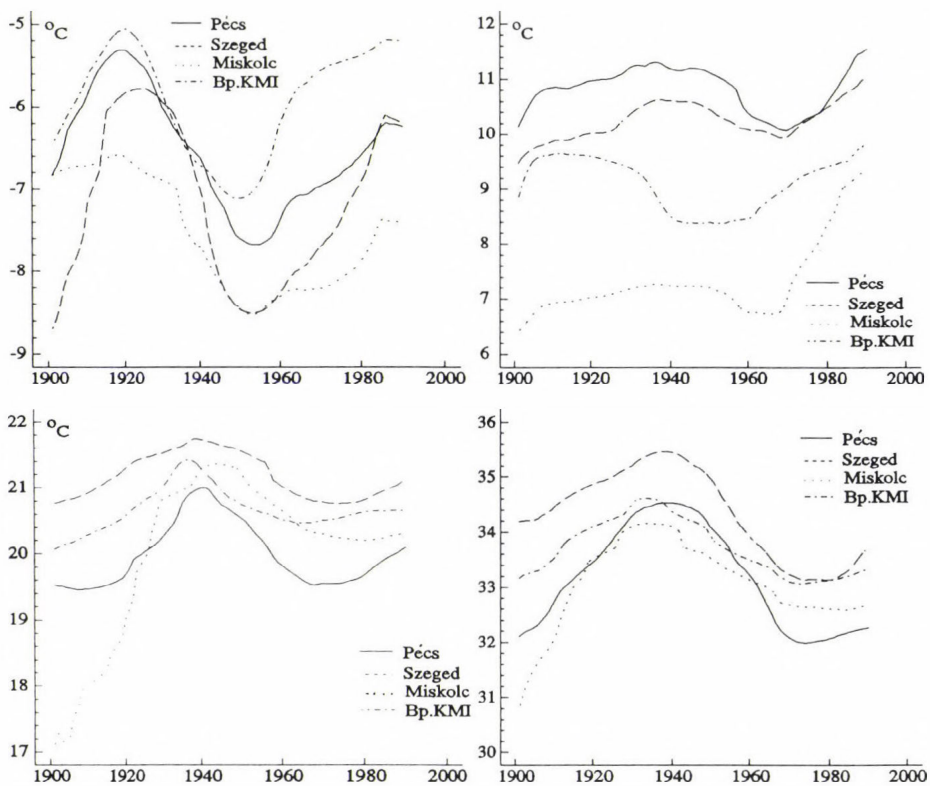

Fig. 2. Time dependent quantiles of daily maximum temperatures for $q = 0.05$ (left) and $q = 0.95$ (right) in winter (top) and summer (bottom).

Table 1. Slopes and test statistics for a linear trend analysis in winter

Station	Slope	Test statistic
Seasonal mean of daily minimum temperature		
Pécs	-0.0127	-1.05
Szeged	-0.0084	-0.62
Miskolc	-0.0126	-0.91
Budapest KMI	+0.0063	+0.56
Seasonal mean of daily maximum temperature		
Pécs	-0.0142	-1.17
Szeged	+0.0022	+0.18
Miskolc	-0.0003	-0.03
Budapest KMI	+0.0018	+0.17

Table 2. Slopes and test statistics for a linear trend analysis in summer

Station	Slope	Test statistic
Seasonal mean of daily minimum temperature		
Pécs	-0.0143	-2.88*
Szeged	-0.0277	-5.15*
Miskolc	-0.0133	-3.10*
Budapest KMI	+0.0082	+1.86
Seasonal mean of daily maximum temperature		
Pécs	-0.0017	-0.23
Szeged	-0.0032	-0.49
Miskolc	+0.0251	+2.81*
Budapest KMI	-0.0052	-0.81

Asterisk shows significant linear trend at a 5% level

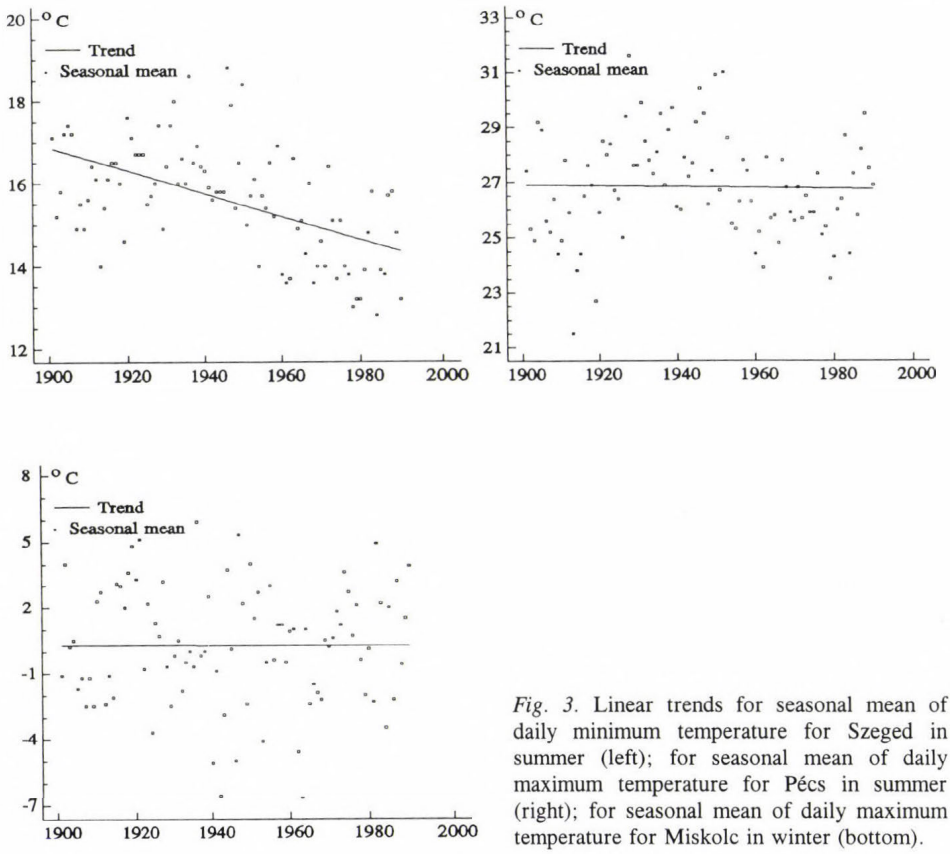

Fig. 3. Linear trends for seasonal mean of daily minimum temperature for Szeged in summer (left); for seasonal mean of daily maximum temperature for Pécs in summer (right); for seasonal mean of daily maximum temperature for Miskolc in winter (bottom).

4. Summary

A method to estimate time dependent quantiles of a variable has been presented. The procedure does not need any specifications on the probability distribution, the unique assumption is its smooth variation in time, which seems certainly reasonable on a climatic scale. An important aspect of the procedure is that bandwidth, a key element of the method, is optimized directly for quantiles and not for distribution functions.

An application for daily maximum and minimum temperatures in Hungary illustrates that high and/or low quantiles characterizing extremes may present considerably variations when conventional trend estimates do not show statistically significant changes.

Acknowledgement—Research leading to this paper has been supported by grant from Hungarian Science Foundation OTKA T025803.

References

Duin, R.P.W., 1976: On the choice of smoothing parameters for Parzen estimators of probability density functions. *IEEE Trans. Comput. C-25*, 1175-1179.

Fan, J., 1992: Design-adaptive nonparametric regression. *J. Am. Statist. Ass. 87*, 998-1004.

Gumbel, E.J., 1958: *Statistics of Extremes*. Columbia Univ. Press, New York.

Koenker, R. and *Bassett, G.S.*, 1978: Regression quantiles. *Econometrica 46*, 107-112.

Leadbetter, M.R., Lindgre, G. and *Rootzen, H.*, 1983: *Extremes and Related Properties of Random Sequences and Processes*. Springer-Verlag, New York.

Magee, L., Burbidge, J.B. and *Robb, L.*, 1991: Computing kernel-smoothed conditional quantiles from many observations. *J. Amer. Stat. Assoc. 86*, 673-677.

Molnár, K. and *Mika, J.*, 1997: Climate as a changing component of landscape: recent evidence and projections for Hungary. *Z. Geomorph. N.F. Suppl.-Bd. 110*, 185-195.

Nadaraya, E.A., 1964: On estimating regression. *Theory Probab. Applic. 15*, 134-137.

Parzen, E., 1962: On the estimation of probability density functions and mode. *Ann. Math. Statist. 33*, 1065-1076.

Rosenblatt, M., 1956: On some nonparametric estimates of a density function. *Ann. Math. Statist. 27*, 832-837.

Tiago de Oliveira, J., 1986: Extreme values and meteorology. *Theor. Appl. Climatol. 37*, 184-193.

Watson, G.S., 1964: Smooth regression analysis. *Sankhya Ser A 26*, 359-372.

Zheng, X. and *Basher, R.E.*, 1999: Structural time series models and trend detection in global and regional time series. *J. Climate 12*, 2347-2358.

IDŐJÁRÁS

Quarterly Journal of the Hungarian Meteorological Service
Vol. 104, No. 1, January–March 2000, pp. 53–59

On the diurnal variation of noctilucent clouds

Wilfried Schröder

Geophysical Station, Hechelstrasse 8, D-28777 Bremen, Germany

(Manuscript received 15 January 1999; in final form 16 September 1999)

Abstract—In a review (Meteorologische Rundschau, 1966, p. 26-27) the author suggested to make more accurate distinctions between "appearance" (in German Häufigkeit) and "brightness" (in German Helligkeit). The author analyses some arguments which were in favor of the daily variation of noctilucent clouds (NLC). It can be shown that there is no remarkable diurnal variation of noctilucent clouds. Earlier observations (1885–1897) make no difference between brightness and appearance, therefore it seems that noctilucent clouds have been detected more after midnight. Recent observations for the total noctilucent cloud period (May–August) do not support this earlier result in general. On the other hand recent data (1985–1997) show a little preference of the clouds after midnight. More studies are necessary for this complex.

Key-words: noctilucent clouds, diurnal variation, mesospheric circulation.

1. Introduction

In the last part of *Jensen et al.* (1989) describe and discuss the diurnal variation of noctilucent clouds as recorded by visual observations. It seems to be useful to make a more careful overview of the ground based data which have been sampled during the last 100 years. Furthermore, an insight into the general problems associated with visual data may be useful for further interpretations (see *Fig. 1* as an example of a noctilucent cloud).

Noctilucent clouds were first observed in Germany in 1885, two years after the great Krakatoa volcanic event of August 1883. Around this event anomalous twilight phenomena were observed and the attention was drawn to these atmospheric processes (see *Gadsden* and *Schröder*, 1989). Originally, people spoke of "glowing clouds" or "silvery clouds". It was probably *O. Jesse* who introduced the term "noctilucent clouds" (Leuchtende Nachtwolken). *Jesse*, who was then active at the Berlin Observatory, also performed the first photographic measurements of the clouds (*Archenhold*, 1928).

With the "Vereinigung der Freunde der Astronomie und kosmischen Physik", a German society of friends of astronomy, a working group was formed under the leadership of Archenhold, Foerster and Jesse with the goal of observing noctilucent clouds. They worked mostly during 1889–1899. More or less sporadic observations were made in Europe and USSR up to the end of the Second World War. More systematic surveillance of these phenomena has been made only since the International Geophysical Year (IGY, 1957) in different parts of the world.

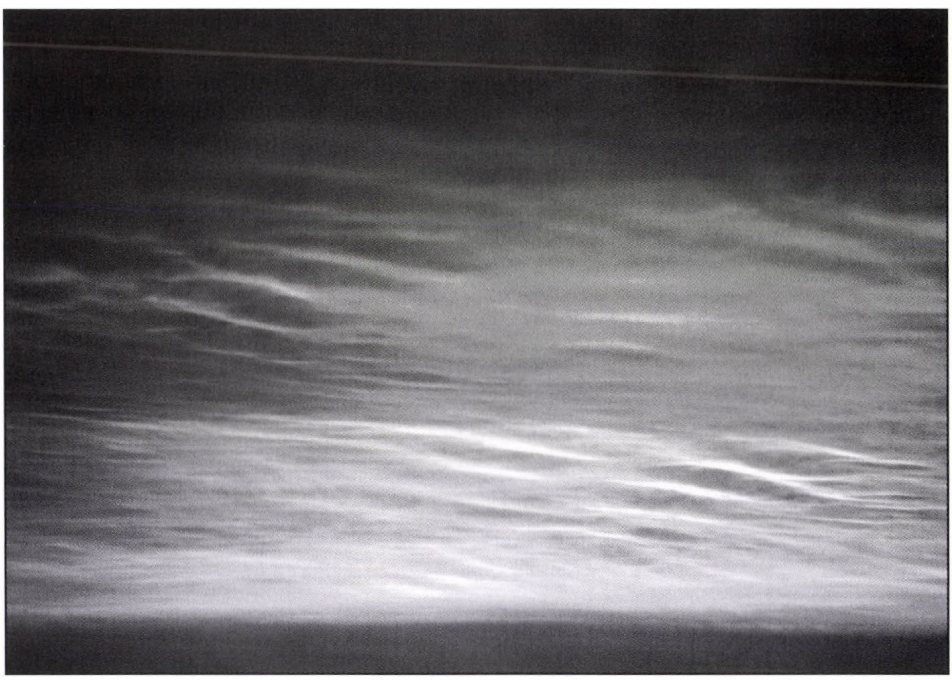

Fig. 1. Noctilucent clouds.

The observations are predominantly visual but there are many photographs and other special measurements too. Taken as a whole, these data have allowed no clear understanding of the complex problem of noctilucent clouds, mainly because of their sporadic nature. This includes the various climatological aspects, i.e., the diurnal and seasonal variation.

2. *Observations of diurnal variation of NLC*

In their last section *Jensen et al.* (1989) discuss the diurnal variation of noctilucent clouds. It seems to be necessary to make a more accurate distinction between the terms "brightness" and "appearance". For visual observations, a scale of noctilucent cloud intensity exists; it has the following five points:

(1) very weak NLC, barely visible against the background of the twilight sky, detected only through very careful examination of the sky;

(2) NLC easily detected, but having low brightness;

(3) NLC clearly visible, standing out sharply against the twilight sky;

(4) very bright;

(5) NLC extremely bright and noticeably illuminate objective facing them.

In many papers diurnal variation was reported in terms of "first sightings" at night and this may possibly have led to the conclusion that the clouds are more frequent after midnight than before. For instance, *Archenhold* (1928) reported: "In 1889–1894, the clouds were observed only 6 times before, but 33 times after midnight". At first *Vestine* (1934) accepted this result, and some decades later *Ludlam* (1957) wrote: "Except in very intense displays, the clouds have been seen more frequently after than before midnight...". A more careful examination of the various data was made later by *Fogle et al.* (1965) and by *Schröder* (1968a,b). It was found that 83% of the North American displays and 60% of the displays over the USSR during the IGY (1957–1958) were first seen before midnight. Furthermore, *Pavlova* (1962) reported that the total number of occasions of the observations of noctilucent clouds was 1.56 time greater in the morning than in the evening twilight. These data relate to the times of first "sighting" (detection by visual observations on each night).

If we look at the "brightness" of the noctilucent clouds, a difference can be pointed out. In one of his first analyses *Jesse* (1890) reported on the variation of brightness of the clouds that "we found an increased brightness of all noctilucent clouds in the morning hours". This was the first report of increasing brightness of noctilucent clouds during the morning hours and this effect has been confirmed in many notes after 1889. The fact that noctilucent clouds are generally brighter and most widespread after midnight may account for the differences found between the earlier and more recent studies on the daily variation of noctilucent cloud frequency (*Fogle* and *Haurwitz*, 1966; *Schröder*, 1968a).

Using the visual estimation of noctilucent cloud brightness, it should be noted that the clouds are usually very patchy, and observers often note the intensity of the bright patches in the display. For visual observation the structure in noctilucent clouds has been classified into four different types (*Gadsden* and *Schröder*, 1989):

I. Veils; II. Bands; III. Billows (or waves); IV. Whirls.

It is possible that in complex displays all four forms are observed simultaneously. The genesis of these formations shows remarkable differences in brightness and lifetime, therefore, visual observations very often report the "brightness" of the clouds as a general term, rather than referring to the different structures. Generally it has been reported by observers that noctilucent cloud brightness (and their different morphological forms I–IV) change considerably during the time of observation.

Table 1 and *2* (cf. also *Fig. 2* for the data of 1991–1995) present a summary of visual estimations of noctilucent clouds based on reports received from regular meteorological stations and individual observers. In general the brightness is reported in the 1–5 scale of intensity described above. It must be considered that the notification of brightness is related to different parts of a display; the clouds are mostly patchy, therefore, general brightness estimation is impossible by visual observations (cf. *Kosibowa* and *Pyka*, 1973, 1979; *Schröder*, 1968b).

Table 1. Variation of brightness of noctilucent cloud displays (1-5 scale classification)

	Time of observations (local time)									
Intensity	22:00 22:30	22:30 23:00	23:00 23:30	23:30 24:00	00:00 00:30	00:30 01:00	01:00 01:30	01:30 02:00	02:00 02:30	02:30 03:00
1	9	6	4	9	6	4	2	4	7	3
2	12	14	12	9	12	13	12	13	13	8
3	3	5	5	9	7	3	9	10	9	1
4	2	2	2	2	4	4	1	8	3	2

The conclusions of Table 1 and 2 are the same as have been reported by earlier observers: (a) in general the noctilucent cloud displays show a variation of brightness; (b) most of the clouds are noted after midnight with the intensity 3–5; (c) maximum before local midnight is not found. Intensity 1–4 have been observed for all different forms of the clouds. Intensities 4 and 5 were very often associated with the forms IIa (bands with diffuse edges), IIIa (billows/waves consisting of straight and narrow, sharply outlined parallel short bands), IIIb (wave-like structure with undulations in the short-bands) and IVb (whirls having the form of a simple band of one, or several bands with a radius of curvature of 3–5°).

Table 2. Brightness of noctilucent clouds detected by visual observations (German and Polish data)

Date of display	Intensity		Date of display	Intensity		Date of display	Intensity		Date of display	Intensity	
	before midnight	after midnight		before midnight	after midnight		before midnight	after midnight		before midnight	after midnight
21.07.1960	I, II		03.07.1966		I/II	12.07.1968	I^+	II, III, I^+	24.06.1972	I	
07.06.1962	II	III, IV	04.07.1966		IV	14.07.1968	I, III	II, IV	28.06.1972		II, III
09.06.1962	II, III	I-IV	05.07.1966		I, IV	21.07.1968		IV	02.07.1972	IV, II	
27.07.1963	II		07.07.1966		II	22.07.1968	I, II (III-V^+)	III-V^+	06.07.1972	II, III	II, I
29.07.1963	II, I		08.07.1966		II	24.07.1968	II, III $(III)^+$	III	22.07.1972	II	II
09.06.1964	II	II-IV	15.07.1966	II		27.07.1968	I, II, III	III^+	04.08.1972	I	II
16.07.1964	I, II		17.07.1966	I, II		28.07.1968	II, III	V^+	07.06.1976	I	III/IV
20.07.1964	II, I		01.06.1067	II	IV/III/II	30.07.1968		III-I	09.06.1976		I
04.05.1965	I, II		16.06.1967	I	I^+	04.08.1968	I, $(IV)^+$	IV^+	17.06.1976		I/II
07.07.1965	II	IV-I	04.07.1967	II	II-IV, I	05.08.1968		IV	21.06.1976	I, IV	III/IV
24.07.1965	II	III-IV-I	16.07.1967		IV, III (V^+)	14.05.1971	II	I, II-III	23.06.1976	III	I, II
20.05.1966	II - I		18.07.1967	II	III, II^+	19.05.1971	I-II		01.07.1976	I, II, II	II, III, IV
22.05.1966	I-II		07.05.1968		I-II	23.05.1971	II-III-VI		05.07.1976	I	I
02.06.1966	II	III-IV	26.05.1968		II	25.06.1971		II	10.07.1976	II, III	III
09.06.1966	II/I	I, II, IV	22.06.1968	I, II, III		26.06.1971		I	02.07.1977		I, II, III
10.06.1966	III/I	II-IV	23.06.1968	III, IV	III	27.06.1971		IV-II-I	07.06.1977	II, IV	IV, III, I
15.06.1966	I, III	I-IV	25.06.1968	I	II	02.07.1971	II	III-I	13.06.1977	I, II, III	III, II, I
18.06.1966		III	27.06.1968		I/II, II^+	04.07.1971	I-II	III-II-I	19.06.1977	I-II	II-I
23.06.1966		II/IV	29.06.1968		I, II, II, III^+	08.07.1971	I-II	II-I	23.06.1977	II, I, IV	III-II-I
26.06.1966	I	I	30.06.1968	I, II		16.07.1971		I-II, II-III	28.06.1977	III-II-	
27.06.1966		III	01.07.1968	I, II	IV^+	17.07.1971	I-II-III		30.06.1977	I, II, III, IV	
30.06.1966	II, I	IV	05.07.1968	I-IV		21.06.1972	II-IV	IV/I	04.07.1977	II, III	
02.07.1966	III	III	09.07.1968			23.06.1972	I-II	II, III, I	10.07.1977	I-II	III-II-I

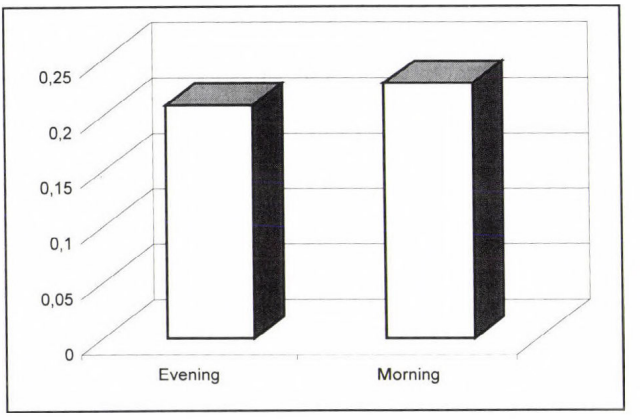

Fig. 2. Relative rate of noctilucent clouds for the periods before and after local midnight for the observations gathered in the years 1991 to 1995 (German data).

It seems to be useful to comment further on the visual data. Most of the displays showed a variation of brightness during the observation epoch, i.e., no display showed "constant" brightness. Because of the variation during the night and/or in twilight, we must consider some subjective aspects and the adaptability of vision of the observer during darkness. During the evening (and morning) twilight the human eye cannot adjust fully to lower illuminations and

It seems to be useful to comment further on the visual data. Most of the displays showed a variation of brightness during the observation epoch, i.e., no display showed "constant" brightness. Because of the variation during the night and/or in twilight, we must consider some subjective aspects and the adaptability of vision of the observer during darkness. During the evening (and morning) twilight the human eye cannot adjust fully to lower illuminations and is less capable of detecting low contrast forms of noctlilucent clouds against the sky background. It would be useful to continue the visual observations of noctilucent clouds, including ground-based data and measurements, paying more attention to the variability of the different forms.

During recent decades the relationship between increased airglow, noctilucent clouds and the influx of cosmic dust has been discussed (*Gadsden* and *Schröder*, 1989). Noctilucent clouds appear at nearly the same time as the May and June increase of meteor streams (e.g., Aquarids, Arietids and Zeta Perseids). The cloud period diminishes shortly after the great injection of August Perseids. In general, the meteor flux is only one possible factor in the development of noctilucent clouds; the other is the condensation of ice particles in the NLC-Zone or at ions detected in the height. But, indeed, the observed diurnal variation in brightness of increased airglow is of interest.

Considering the conclusions of *Jensen et al.* (1989) and the noctilucent cloud and increased airglow data, it would be valuable to continue this research in the future.

The diurnal variation of noctilucent clouds has been noted in general terms. Further research should aim to present more details on the dependence of brightness of noctilucent clouds on oservational (local) time and to make some possible refinements, including the assumptions of *Jensen et al.* (1989).

3. Conclusion

From the available data no clear conclusions are possible. Some of the observations indicated an increased brightness of the NLC-display after midnight but it seems to be useful to get more data for analyses. In general, the old data of *Jesse* (1890) showed an increase after midnight, but they are different from the "frequency of appearance". Therefore, presently we would say that the brightness of NLC showed a variation during the observation time, although the question of frequency of occurrence at night is now an unsolved problem.

Acknowledgement—I am grateful to *U. Freitag* and the referees for their helpful comments.

References

Archenhold, F. S., 1928: Die leuchtenden Nachtwolken und bisher unveröffentlichte Messungen ihrer Geschwindigkeit. *Weltall 27*, 137-144.

Fogle, B., Capman, S. and *Echols, C.*, 1965: Noctilucent clouds—a survey with special reference to recent observations. *Univ. of Alaska, UAG-R*, 162.

Fogle, B. and *Haurwitz, B.*, 1966: Noctilucent clouds. *Space Sci. Rev. 6*, 279-340.

Gadsden, M. and *Schröder, W.*, 1989: *Noctilucent Clouds*. Springer-Verlag, New York.

Jensen, E., Thomas, G.E., and *Toon, O.B.*, 1989: On the diurnal variation of noctilucent clouds. *J. Geophys. Res. 94*, 14.693-14.699.

Jesse, O., 1890: *Untersuchungen über die sogenannten leuchtenden Nachtwolken*. Sitz-Ber. Preuß. Akad. Wiss. Berlin, 1031-1044.

Kosibowa, S. and *Pyka, J.L.*, 1973: Mesospheric clouds visible in Poland during 1971. *Acta Geophys. Pol. XXI*, 168-178.

Kosibowa, S. and *Pyka, J.L.*, 1979: Mesospheric clouds observed in Poland during 1977. *Acta Geophys. Pol. XXVII*, 187-193.

Ludlam, F.H., 1957: Noctilucent clouds. *Tellus 9*, 341-364.

Pavlova, T.D., 1962: *Preliminary Statistical Data on the Frequency of the Appearance of Noctilucent Clouds in the Year 1959* (in Russian). Trudy covescan. po. serebristym oblakam, Tallinn.

Schröder, W., 1968a: Zur Charakteristik der Leuchtenden Nachtwolken während der Jahre 1963-1967. *Gerlands Beitr. Geophys. 77*, 441-448.

Schröder, W., 1968b: Analyse der täglichen Häufigkeit der Leuchtenden Nachtwolken. *Meteorol. Rdsch. 21*, 28-30.

Vestine, E.H., 1934: Noctilucent clouds. *J. Roy. Astron. Soc. Can. 28*, 249-272 and 303-317.

BOOK REVIEWS

Ernő Mészáros: **Fundamentals of Atmospheric Aerosol Chemistry**. Akadémiai Kiadó, Budapest, 1999. 308 pages, 11 chapters, several figures and tables, more than 600 references.

Aerosol particles are important constituents of the atmosphere. Although, they were already known by the scientists of the last century, their intensive study was started in the 1950s. These particles play determining role in cloud and precipitation formation, solar radiation transfer, and visibility. Nowadays, the questions of global warming give a special emphasis on aerosol research as the aerosol particles may cause negative radiative forcing, partly compensating the effect of greenhouse gases. They are also involved in chemical transformations like the ozone removal in the stratosphere. All these effects depend on the physical and chemical properties of the particles.

Professor Mészáros' book introduces the reader into the science of atmospheric aerosol step by step, overviewing the origin of the particles, their types and atmospheric roles. The book consists of 11 chapters. The first chapter is an introductory one where the reader may get acquainted with the basic terms of aerosol science and with the basic physical properties and processes related to the particles. The second chapter covers the chemical properties. It also describes the most widespread sampling and analytical techniques. A short subchapter is devoted to a quickly developing field, to the ground-, aircraft- and satellite-based remote sensing of atmospheric aerosol.

The next three chapters present the different ways of aerosol formation: chemical reactions, burning processes, disintegration of the surface, and release from the biosphere. Having the particles in the atmosphere, they can be classified according to their chemical composition. One of the groups is that of the water soluble inorganic particles which, among others, includes the sea salt particles and the different sulfate and nitrate containing ones. Chapter 6 discusses their size distribution, as well as their spatial and temporal distributions over the globe.

Metal containing aerosol particles form the next group which is introduced in Chapter 7. They, as catalysts, play an important regulatory role in the chemical transformations in the atmosphere. A part of them, the so-called heavy metals are also known by their adverse effects on the living environment. Lead, a high amount of which is emitted by the gasoline driven vehicles, has got a special public attention during the last decades because of its harmful health effect. However, the lead pollution is not only the problem of our era, it was also high during the Greek and Roman cultures, as we can learn from a short subchapter.

Carbonaceous particles have got into the focus of aerosol science only recently. Due to their optical properties they play an important role in the radiation balance of the Earth, but they are also involved in the cloud and precipitation formation. Chapter 8 presents their size distribution as well as their spatial and temporal distributions. In the case of organic aerosol, the chapter also discusses its certain subclasses (aliphatic and aromatic compounds, organic acids, etc.).

Cloud droplets form on certain type of aerosol particles (condensation nuclei). Thus, the physical and chemical nature of aerosol play a significant role in the cloud/precipitation formation. In the cloud and precipitation droplets chemical transformations may occur. Evaporation of the droplets may release particles again, while the precipitation may wash them out to the surface. This sort of deposition may contribute to serious environmental problems like acidification. All these processes are overviewed in Chapter 9.

The next chapter discusses the effect of atmospheric aerosol on visibility and climate. The cooling effect of the aerosol particles is still one of the most uncertain questions of the global climate change research.

In the previous chapters the emphasis was on the tropospheric aerosol. The stratosphere differs from the troposphere in several aspects. In the stratosphere the residence time of the particles is much longer and thus they are able to cause global effects. This last chapter of the book reviews the origins and effects of the stratospheric aerosol, also mentioning the effect of the huge volcanic eruptions and the heterogeneous chemical reactions causing ozone loss in the stratosphere (formation of the "ozone hole").

The book is rich in measurement data which are presented in well designed figures and tables (more than 70 figures and almost 50 tables). In the enormous reference list (around 600 items) the reader can find the sources of the data, and further readings if he/she is interested in more details. The well-structured volume, considered as an introduction to the subject, can be recommended for both graduate students and research workers in earth and environmental science. The author is a skilled writer of scientific books, and his style also makes the subject understandable for all educated persons interested in atmospheric environment.

László Haszpra

N. Rescher: **Predicting the Future. An Introduction to the Theory of Forecasting.** State University of New York Press, Albany, 1998. 315 pages, five parts, 14 chapters, 4 tables.

W. A. Sherden: **The Fortune Sellers. The Big Business of Buying and Selling Predictions.** John Wiley & Sons, New York, 1998. 308 pages, 9 chapters, 54 figures.

Not only weather but almost everything that touches our life is filled with a kind of uncertainty that grows as we try to look weeks, months and years into the future. On a daily basis, we are showered with all types of predictions. Meteorological predictions (weather forecasts and climatological predictions) represent only a very small part of the multibillion-dollar and day-by-day growing industry of selling and buying predictions.

History is full of all sorts of wild schemes aimed at figuring out the future. Marcus Tullius Cicero (106-43 BC), statesman and poet, ancient Rome's greatest orator stated that the Roman government relies on two basic principles: ritualism and divination. In his work from 44 BC, "De Divinatione" (On Divination, i.e., supernatural insight into the future) Cicero presents an extended discussion of pluses and minuses of divination, eventually declaring that liabilities far outweight the benefits.

Predicting the Future by philosopher of science *Nicholas Rescher*, as he states "is the first book on the theory of prediction-in-general since Ciceros's De Divinatione". The author presents a general theory of prediction: its basic principles, methodology, promises and problems. Rescher also sorts out the difference between prediction (falsifiable or verifiable statements) and forecasts (unfalsifiable or unverifiable statements). He discusses the relationship between prediction and probability, as well as the theory of knowledge and the nature of reality. Rescher presents different sorts of methodology ranging from completely unformalised judgements (essentially personal options) to very formal schemes based on the laws of natural sciences and mathematical modeling.

As Rescher says, the mere correctness of a prediction is neither necessary nor sufficient to label either the prediction or the predictor "good". Equally, failure of the prediction does not necessarily mean that it or the method was bad. Discussing barriers of predictability ranging from instability and chaos to free will, innovation and quantum indeterminancy, Rescher provides reasons why we will never attain the nirvana of perfect foreknowledge.

While Nicholas Rescher focuses in his book on the ontology and epistemology of scientifically based prediction methods, *William Sherden*, financial and strategic planning consultant of multinational coorporations, casts a critical eye on seven areas in wich forecasts of the future have become big business: meteorology, macroeconomics, finance, demography, technology, organizational

planning and futurology—the future of the future itself. With a combination of anecdotes, examples, historical and statistical facts the book attempts to separate predictions one can count on from vague, personal opinions and guesswork. Sherden demonstrates the reasons why reliable forecasts of the weather more than about 10 days ahead will remain in the realm of fantasy, regardless of whatever advances technology may bring. The book also traces the fascinating tale of how profits can actually be made from stock-market predictions—but not by investing. Based upon observations made as business consultant, Sherden presents a compelling argument for the case that "there is just no future in the past". To sum it up, Sherden offers an informal, almost journalistic tour through the minefields of the predictive enterprise as it is practised today.

Taken together, these two books constitute a very good introduction of the state of the predictive arts. The *Fortune Sellers* tells it like it is about the way prediction is practised in the worlds of commerce and industry, while *Predicting the Future* lays down a solid philosophical and logical foundations of making predictions. Bad news is that both authors conclude that perfect prediction is impossible. According to Sherden's estimations, we annually get at least $200 billion of mostly erroneous future predictions from professional prognosticators. Both authors give us the clearest possible explanation why it happens.

Good news for meteorologists is formulated by William Sherden as follows: "Weather forecasting is the most successful of all the future-predicting professions. ... In fact, meteorology is the only forecasting profession that employs proved laws of nature to make predictions. ... Meteorology is also the only forecasting profession among the fortune sellers that has shown clear signs of improvement."

György Gyuró

ATMOSPHERIC ENVIRONMENT

an international journal

To promote the distribution of Atmospheric Environment *Időjárás* publishes regularly the contents of this important journal. For further information the interested reader is asked to contact *Prof. P. Brimblecombe*, School for Environmental Sciences, University of East Anglia, Norwich NR4 7TJ, U.K.; e-mail: atmos_env@uea.ac.uk

Volume 34 Number 1 2000

NOTES TO CONTRIBUTORS OF *IDŐJÁRÁS*

The purpose of the journal is to publish papers in any field of meteorology and atmosphere related scientific areas. These may be

- reports on new results of scientific investigations,
- critical review articles summarizing current state of art of a certain topic,
- shorter contributions dealing with a particular question.

Each issue contains "News" and "Book review" sections.

Authors may be of any nationality, but the official language of the journal is English. Papers will be reviewed by unidentified referees.

Manuscripts should be sent to
Editor-in-Chief of IDŐJÁRÁS
P.O. Box 39
H-1675 Budapest, Hungary

in three copies including all illustrations. One set of illustrations has to be of camera ready quality, the other two might be lower quality.

Title part of the paper should contain the concise title, the name(s) of the author(s), the affiliation(s) including postal and E-mail address(es). In case of multiple authors, the cover letter should indicate the corresponding author.

Abstract should follow the title, it contains the purpose, the data and methods as well as the basic conclusion.

Key-words are necessary to help to classify the topic.

The text has to be typed in double spacing with wide margins. Word-processor printing is preferred. The use of SI units are expected. The negative exponent is preferred to solidus. Figures and tables should be consecutively numbered and referred to in the text.

Mathematical formulas are expected to be as simple as possible and numbered in parentheses at the right margin. Non-Latin letters and hand-written symbols should be indicated and explained by making marginal notes in pencil.

Tables should be marked by Arabic numbers and printed in separate sheets together with their captions. Avoid too lengthy or complicated tables.

Figures should be drawn or printed in black and white, without legends, on separate sheets. The legends of figures should be printed as separate list. Good quality laser printings are preferred as master copies.

References: The text citation should contain the name(s) of the author(s) in Italic letter and the year of publication. In case of one author: *Miller* (1989), or if the name of the author cannot be fitted into the text: *(Miller,* 1989); in the case of two authors: *Gamov* and *Cleveland* (1973); if there are more than two authors: *Smith et al.* (1990). When referring to several papers published in the same year by the same author, the year of publication should be followed by letters a,b etc. At the end of the paper the list of references should be arranged alphabetically. For an article: the name(s) of author(s) in Italics, year, title of article, name of journal, volume number (the latter two in Italics) and pages. E.g. *Nathan, K.K.,* 1986: A note on the relationship between photosynthetically active radiation and cloud amount. *Időjárás 90,* 10-13. For a book: the name(s) of author(s), year, title of the book (all in Italics except the year), publisher and place of publication. E.g. *Junge, C. E.,* 1963: *Air Chemistry and Radioactivity*. Academic Press, New York and London.

The final version should be submitted on diskette altogether with one hard copy. Use standard 3.5" or 5.25" DOS formatted diskettes. The preferred word-processors are WordPerfect 5.1 and MS Word 6.0.

Reprints: authors receive 30 reprints free of charge. Additional reprints may be ordered at the authors' expense when sending back the proofs to the Editorial Office.

More information: gmajor@met.hu
Information on the last issues:
http://www.met.hu/firat/ido-e.html

Published by the Hungarian Meteorological Service

Budapest, Hungary

INDEX: 26 361

HU ISSN 0324-6329